The Dissertation Committee for Mengqi Yuan Certifies that this is the approved version of the following dissertation:

Additive Manufacturing of Laser Sintered Polyamide Optically Translucent Parts

Committee:

David L. Bourell, Supervisor

Joseph J. Beaman

Wei Li

Carolyn C. Seepersad

Maria C. Juenger

Additive Manufacturing of Laser Sintered Polyamide Optically Translucent Parts

by

Mengqi Yuan, B. E.; B. E.; M. S. E.

Dissertation

Presented to the Faculty of the Graduate School of

The University of Texas at Austin

in Partial Fulfillment

of the Requirements

for the Degree of

Doctor of Philosophy

The University of Texas at Austin

December 2013

Acknowledgments

I would like to express my sincere gratitude to Dr. Bourell for being a considerate and motivating advisor. This dissertation would not have been possible without his valuable support, guidance and encouragement. Deep gratitude is also given to Dr. Beaman, Dr. Li, Dr. Seepersad, and Dr. Juenger for their valuable advice and patience as my committee members.

I would like to thank Mark Philips who provided assistance with the laser sintering process and device maintenance; I could not finish the experiments without his kind and experienced advice and considerations. I would like to thank Rosalie Foster for her excellent administrative skills. I would also like to thank Fred, Danny, and Scott for their suggestions and guidance in manufacturing process.

I would like to thank Abhimanyu, Jevons, Mu, Ellyn, Courtney, Nicole, and Steven for their support and help. Special thanks go to Lars and Vikram, who help me significantly in AutoCAD document setup and HiQ SinterStation experiment preparations.

I would like to thank Billy, Jeff and Don from Harvest Technologies for their help and guidance in the SL processing, surface finish, etc. Special thanks go to David Leigh and Ben Fulcher for their valuable experience, advice, and thoughtful conversations on laser sintering and research in general.

Dedication

I dedicate this dissertation to my lovely parents. They have always encouraged me to pursue my dreams and supported my decisions. I would like to thank them and show them my love from the bottom of my soul and the depths of my heart. Great thanks to my grandparents, and other relatives in my family for their concern and care.

I would like to dedicate this dissertation to my sweet girl friends Yunping Fei, Xuanqi Zhang, Zoe Zhang, who provided me with a strong shield of love and prevented sadness from enter inside. I really enjoyed hanging out with them. Special thanks to my lovely roomie Keren. She cooked delicious food, supported and helped me around when I was too busy. Huge thanks to Tang Lu, Qian Shao, Qing Ye, Weiky Liu and Wei Jiang. Without your love and care I could not finish this work.

I want to dedicate this work to my officemates (Xiaobin Xu, Chao Liu, Jianhe Guo, Fede), and TAs for ME 136 Lab, Felipe, Jevons, Emre, and Wentao for their support and care.

Additive Manufacturing of Laser Sintered Polyamide Optically Translucent Parts

Mengqi Yuan, Ph. D

The University of Texas at Austin, 2013

Supervisor: David L. Bourell

Lithophane is a translucent image created by varying the plate thickness; the image is observed using a back lit light source. Software Bmp2CnC linearly converts the black and white image grayscale into the thickness, thus generates CAD file and lithophane is fabricated by additive manufacturing machines. Additive manufacturing makes highly complex lithophane fabrication possible. It is a convenient, rapid, green, design-driven, and high precision way to make lithophanes, and no post processing is needed.

Optical properties of laser sintered polyamide 12 translucent additive manufactured parts were analyzed in this dissertation. First, selected optical properties of laser sintered polyamide 12 blank plates under different monochromatic light and white light were investigated and applied in production of laser sintered lithophanes to achieve better performance. A spectrophotometer was used to measure the transmittance of visible light through laser sintered polyamide 12 plates as a function of plate thickness. The transmittance decreased with increasing plate thickness according to a modified

Beer-Lambert Law, and it varied significantly depending on the monochromatic wavelength. Monochromatic LEDs were used to assess the wavelength dependence on the transmission and contrast. Highest transmission was observed with green light (540 nm), and poorest transmission was measured for yellow light (560 nm).

Second, several parameters affecting lithophane manufacturing performance were analyzed including lithophane orientation with respect to light source, brightness and contrast versus plate thickness and grayscale level, quantized plate thickness correction, surface finish quality, and manufacturing orientation. It was found that brightness was relative to the plate thickness. The contrast was defined by the lithophane grayscale level, which was influenced by sintering layer thickness, plate thickness, and sintering orientation. Thinner sintering layers resulted in more grayscale levels of the image and smaller difference between the theoretical thickness and actual thickness. Relatively larger plate thickness defined greater contrast; however, the plate thickness was limited due to the light transmission. Lithophane quality was largely improved by changing the manufacturing orientation from the XY plane orientation to the ZX/ZY plane orientation. The grayscale level changed continuously when parts were constructed in the z orientation.

Third, other thermoplastic semi-crystalline materials were analyzed for LS optically translucent part production. Last, plates and lithophanes were built using a different AM platform: stereolithography (SL) with Somos® ProtoGen™ O- XT 18420

white resin. Different optical properties and lithophane performance were found and compared with PA 12 parts.

In conclusion, laser sintered polyamide 12 optical properties varied with light wavelength and reached the maximum under green light. When building in the XY plane, thinner layer thickness (0.07 mm) and relative thicker maximum plate thickness (3.81 mm) leaded to higher contrast and greyscale level. Lithophane quality was largely improved when fabricated in the ZX/ZY plane orientation. Lithophanes made from stereolithography were analyzed but showed lower contrast due to the optical property difference of the white resin.

Laser sintered lithophanes serve as an interesting and complex LS industrial application. Optical properties, manufacturing aspects, and other related issues were analyzed and discussed in this dissertation. Future work may include the use of nanocomposites for optimal lithophane performance, and more precise manufacturing processing to improve the lithophane resolution.

Table of Contents

List of Tables

List of Figures

Chapter 1: Introduction

1.1 LASER SINTERING

1.1.1 LS History

Laser sintering (LS) was developed and patented by Dr. Carl Deckard at The University of Texas at Austin in the mid-1980s, under sponsorship of the National Science Foundation (NSF) (Deckard, 1989). The first generation was called 'Betsy' in 1986, with an enclosed electrical box and counter-rotating roller.It worked well for casting patterns. The second generation was named 'Godzilla', which was never built due to the size, weight and prices that were unaffordable for economical production.

'Bambi' was the third generation in 1987 which contained integrated CAD software written by a graduate student Stanley Ogrydziak and more expertise in laser technology and material improvement was provided by Dr. Dave Bourell. SinterStation 2000 was developed in 1992, which was the first modern production machine featuring a 13 inch diameter cylindrical build area. SinterStation 2500, 2500+, and Pro followed with improvement on larger fabrication area, more precise thermal control, and less cost (UT ME website, 2013).

1.1.2 LS Station

LS is an additive manufacturing technology that uses a laser to fuse polymer powder into a mass that has a desired three-dimensional shape. The laser heating results in melting and powder local consolidation. Figure 1 shows the process chain of the laser sintering process (Chua, Leong *et al*., 2003). The laser selectively scans and fuses powder material layer-by-layer on the surface of the powder bed based on the previously generated CAD file, which is always industry-standard STL file format. After one layer is scanned, the powder bed is lowered by one layer thickness, creating a new layer. The process is repeated until the part is completed.

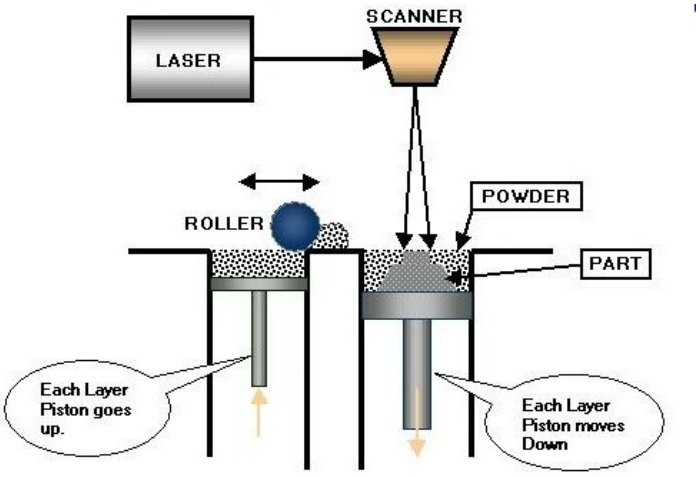

Figure 1: Sketch of the laser sintering process

The experimental work covered in this dissertation is based on the Sinterstation® 2500 and Vangaard HiQ™ by 3D Systems. The SinterStation 2500 had a laser scan speed of 0.5- 2.5 meter/second; for the HiQ SinterStation, the maximum scan speed is 5 meter/second. As shown in Figure 2 below, the build chamber of the machine consists of three powder bins: two feed bins and a part bin where laser sintering occurs. A movable platform contains a radiant heater over each of the bins for powder pre-heating. During machine operation, the platform is lowered so that the heaters are positioned 0.23 m (9 inch) above the powder bed surface. The platform can be raised to facilitate part removal. The center of the heater over the part bin is cut out to allow the laser beam to pass through to the part bed surface. Control of power to the heaters is proportional.

Feedback for the part bin is based on temperature measured with an IR sensor measuring a spot slightly to the rear of center of part bed powder surface. For the feed bins, a thermocouple mounted to the sidewall of the cylinder measures temperature just below the powder surface. The interior of the build chamber, with the platform in the lowered position, is shown in Figure 2 (Diller, *et al*., 2013).

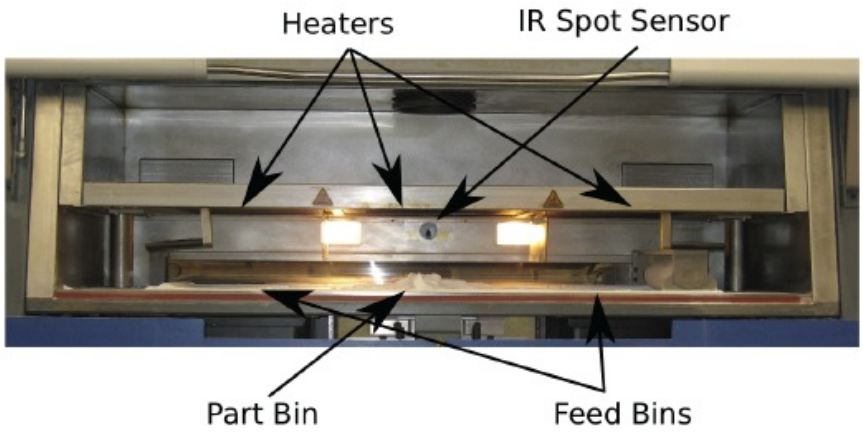

Figure 2: Build chamber of SinterStation 2500

1.1.3 LS Parameters

Many manufacturing parameters are involved during LS process. To achieve the optimal processing quality, these parameters are set differently regarding to powder, machine, property and application needed. Therefore it is of importance to understand the relation between the set up parameters and manufacturing goal. Some of the LS parameters are discussed below.

A. Part bed temperature

For polymer LS, the part bed is heated continuously before the laser scanner moves in its warm up stage. It is heated by the part bed heater mounted on the moveable platform on the top, and the temperature is detected by the IR sensor on the sinterstation sidewall. The part bed is also heated during the LS process to maintain a temperature just lower than the material melting point. Maintaining this relatively high part bed temperature benefits in reducing the laser power during LS as well as part distortion.

The part bed temperature has an effect on the laser sintered part mechanical properties as shown in Table 1 (Yuan and Bourell, 2012) below. Hot spot and cold spots are present in commercial sinterstations, with the thermal variation being around 3-5 °C. Tensile bars built with the same laser power show different mechanical properties (around 15- 20 MPa tensile strength difference, 3-20% elongation difference) due to the part bed temperature difference.

Laser scan power (Watts)	Spot	Tensile strength (MPa)	Elongation (%)
4	Hot spot	39.3	28
	Cold spot	20.4	6.5
10	Hot spot	54.3	28
	Cold spot	41.6	25

Table 1: Mechanical properties of laser sintered tensile bars on different spots with different laser powers, from Yuan and Bourell (2012).

B. Feed bin temperature

Powder in left and right feed bins are heated during the warm-up stage to 40-70 °C lower than part bed temperature, to prevent powder over heating and melting on the high temperature part bed. For the SinterStation 2500, the feed bin surface temperature is monitored by thermocouples mounted on the sidewall of the bin just below the powder surface; For the SinerStation 2500 Pro, feed bin temperatures are monitored by IR spot sensors on the rear sidewall.

C. Fill laser power

The laser fill power should be set to ensure the powder would reach a temperature near the melting point during the laser scan (Gibson and Shi, 1997). The power setting varies with machine and powder types. For polymer powder, the power range is around 20-50 Watts. For metal powder, the power could reach 200-500 watts (Wang *et al*., 2002).

The fill laser power has an effect on the laser sintered part mechanical properties as shown in Table 1 above. The tensile bars built on the same spot have different tensile strength (15-20 MPa variations) and elongation (0-18% variations) due to the change in laser energy. Larger laser power results in higher part bed surface temperature; thus, the polymer behaves like a highly viscous liquid and diffuses more intensely. The porosity can be reduced, and the mechanical properties improve. After laser scanning over a layer, the sintered part temperature drops and diffusion rate decreases, allowing the chains to rearrange to form a nucleus and hence form the whole part layer by layer (Gibson and Shi, 1997). Fill laser power can be calculated as:

$$P = \frac{BS*\rho* D_b*h*[C*(T_m-T_b)+l_f]}{(1-R)} \qquad (1)$$

where BS is the beam speed, ρ is the powder density, D_b is the diameter of laser beam, h is sintering layer thickness, C is the heat capacity, T_m is the melting temperature, T_b is the part bed temperature, l_f is the latent melting heat and R is the reflectivity, the fraction of laser light reflected by the powder.

D. Scan spacing

Scan spacing is the distance between two neighboring parallel scan vectors. If scan spacing is too large, the cross- section might not be completely sintered; if scan spacing is too narrow, the area might be over sintered.

E. Layer thickness

Layer thickness is the distance that part drops for each layer that determines the sinter depth. The range of layer thickness on the SinterStation 2500 and HiQ is 0.0762- 0.5 mm and the default setting is 0.1mm. Increasing layer thickness requires an increase in laser power to maintain successful LS, and has effect on the part surface quality and manufacturing time. For example, if the layer thickness changes from 0.1 mm to 0.0762 mm, the laser power needs to be reduced by 20-30%, and the manufacturing time would increase.

LS technology has many advantages compared to traditional manufacturing methods including the convenience of quickly build complicated customized parts without molding or tooling, especially in aerospace and bio-mechanical areas that need high value, low production parts. Another unique advantage of LS is the ability to create complex geometrical shapes that are impossible to manufacture with other methods. It further does not require assembling afterwards.

1.2 LS MATERIAL AND APPLICATION

1.2.1 LS Material Categories

Polymers, metals, ceramics (including foundry sand) and many kinds of composites are suitable for LS (Kruth *et al*., 2003). Table 2 was made to show examples of different types of LS materials shown below.

	Metal	Ceramic	Polymer
Single component	Ni alloy, Fe, Cu (Tolochko *et al*., 2003), and etc.	SiC, Al_2O_3, $ZiSiO_4$ (Klocke and Wirtz ,1997) and etc.	PA, PC, flux, and etc.
Composites	Ni-alloy-Cu, Fe- Cu, Cu-coated Ni- alloy (Tolochko *et al*., 2003) and etc.	PLA-HA (Taboas *et al*., 2003), Co- Cr (Akova *et al*., 2008) and etc.	PEEK- HA (Tan *et al*., 2003), PA11-MWNT and etc.

Table 2: Category and example of LS materials.
PA: polyamide; PC: polycarbonate; PEEK: polyetheretherketone; HA: hydroxyapatite; MWNT: multiwall nanotubes; PLA: polylactide.

1.2.2 Polymer Laser Sintering

Polymers are widely used in LS. Applications include rapid prototyping, commercial industrial production, tissue engineering ((Tan *et al*., 2005; Leong *et al*., 2003; Williams *et al*., 2005), when blending with ceramics, biodegradable materials (Tan *et al*., 2003), metal (Kruth *et al*., 2005; Song *et al*., 1997), etc.

Polymers are made up of long chain molecules formed primarily by carbon- to- carbon bonds. In some cases like metal- polymer powders, the polymer acts as a binder and the fabrication parameters are mainly dependent on the properties of polymers (Gibson and Shi, 1997).

Thermoplastics are used most in the LS process among all three types of engineering polymers: thermoplastic, thermosetting and elastomer (Douling, 1993). It can be recycled afterwards. Generally used LS polymers include: aluminum filler nylon, carbon filled nylon, Durform® EX black, Durform® EX natural, Durform® FR 100, Durform® HST, flex, glass filled nylon PA 615, glass filled nylon PA 616, nylon11, nylon 12/ Durform® PA, nylon 12 FR/ PA 606 FR, PA 2200 and PA 2210 FR (LaserSintering.com).

There are two kinds of thermoplastics: amorphous and crystalline. Amorphous material has chain molecules arranged in a random manner like in polycarbonate (PC); crystalline material has chain molecules arranged in an orderly structure like nylon. Crystalline and amorphous materials have different properties thus different LS manufacturing parameters (Gibson and Shi, 1997).

Two essential properties that determine the manufacturing processablity of thermoplastic polymers are glass transition temperature T_g and melting temperature T_m. T_g is the temperature where a rapid decrease in elastic modulus occurs (Tobolsky, 1967). Below T_g, polymer is in a glassy state and the molecular motion along the chain is frozen; the molecular motion increases with temperature rises (Tg+30K), causing the modulus to drop. The polymer behaves like a viscous liquid above T_m where chains are all tangled.

T_m and T_g are related with polymer mechanical properties (elastic modulus), specific volume, and other physical properties. Specific volume is the ratio of a substance volume to its mass. The change of specific volume regarding to temperature on different types of materials are shown in Figure 3 below (Gibson and Shi, 1997). It changes greatly for thermoplastic polymers at T_m, which explains why a part made with crystalline polymer shrinks rapidly when cooling down from T_m and uneven cooling results in part distortion.

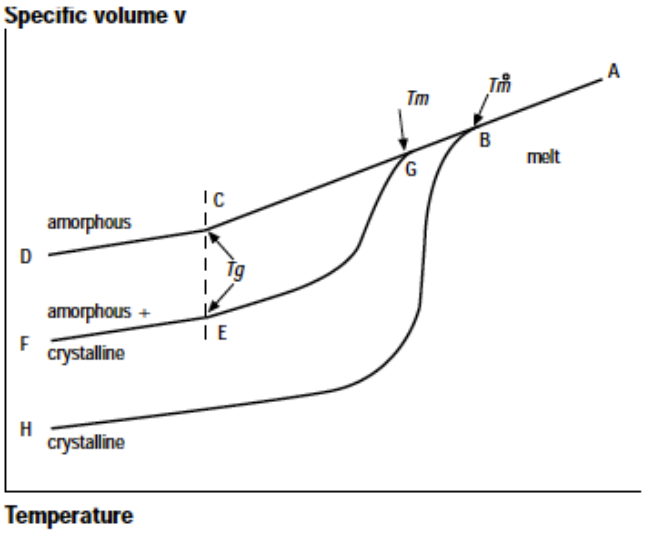

Figure 3: Specific volume versus temperature for polymers.

Thermoplastic material polyamide (PA) 12, also known as Nylon 12, is used in this work for LS. Detailed mechanical and thermal properties are shown in Chapter 2.

1.3 LITHOPHANES

1.3.1 Background

A lithophane is a translucent image created by varying the plate thickness; the image is observed using a back lit light source. It is a design in gray tones (Carney *et al*., 2007; Houze *et al*., 2006). It presents a three-dimensional image that completely different from two dimensional engravings and daguerreotypes that are 'flat' (Carney *et al*., 2007; Houze *et al*., 2006; Jean-Baptiste-Ambroise-Marcellin Jobard, 1858). Laser sintered polyamide 12 lithophane looks blurry with front lit light on as shown in Figure 4a, and the figure is shown remarkably greater contrast with back lit light on in Figure 4b. The photo is a reproduction of Raphael's painting, Agnolo Doni (Raphael, 1507).

Figure 4: Image of the same laser sintered polyamide 12 lithophane with a) front lit light source; b) back lit light source.

The word 'lithophane' derives from Greek 'litho' means stone or rock, and 'phainein' means 'to cause to appear (suddenly)' (Houze *et al*., 2006); from this is derived a meaning for three dimensional image appears suddenly when with a back lit source (Carney *et al*., 2007).

1.3.2 Lithophanes Made with Other AM Technologies

Lithophanes have been made with other rapid prototyping methods including three dimensional printing and fused deposition modeling (FDM) (Suwanorateeb *et al*., 2009; Ahn *et al*., 2004). CNC machine was also used for lithophane production.

Suwanorateeb *et al*. (2009) investigated the feasibility and studied the properties of increased transparency samples fabricated by three dimensional printing (3DP). Polymethyl methacrylate (PMMA) was mixed with maltodextrin binders and used as the raw material for 3DP. The samples were then divided into two groups: infiltration with heat-cured acrylate infiltrant or subjected to binder elimination prior to infiltration. It showed the maximum transmittance (25-30%) was achieved at binder with 10 percent PMMA. Binder elimination prior to infiltration was an essential step in increasing the transmittance, without which the 3DP sample transmittance only increased 1 percent. This is related to the decrease in porosity from infiltration and a generation of strong interfacial bonding between PMMA particles and the acrylate infiltrant material. However, the transmittance range was narrow, which resulted in narrow contrast levels presented on the lithophane.

Ahn *et al*. (2004) analyzed two post-processing techniques to increase the optical transmittance of the part made of ABSi by fused deposition modeling (FDM). ABSi was the name of Stratasys' medical grade thermoplastic ABS. The effect of raised temperature and infiltration of resin in post-processing were studied. The best elevation temperature turned out to be 180°C where transmittance increased by 10%. Resin infiltration followed by surface sanding was the optimal post processing which made the transmittance increase by 16%.

1.4 LIGHT TRANSMISSION

1.4.1 Theory and Modeling

The optical properties of the material are essential for lithophane application as this is critical to define the brightness and contrast. The fraction of incident light transmitted by an optical material depends on losses due to absorption and back reflection (Rose *et al*., 1965). This work we believe represents a first effort to study systematically the optical behavior of LS polyamide 12 as it affects lithophane performance.

The transmittance largely varies with wavelength and materials. As shown in Figure 5 below, the wavelength-dependent relation defining the interaction of light with a solid object is:

$$A_\lambda + R_\lambda + T_\lambda = 1 \qquad (2)$$

where A_λ is the fraction of light absorbed, R_λ is the fraction of light reflected, and T_λ is the fraction of light transmitted, and λ is the light wavelength. R_λ is related with the refractive index *n* which is a dimensionless number describing the light propagation through a medium. It varies with material, temperature and wavelength:

$$R = \left(\frac{n-1}{n+1}\right)^2 \qquad (3)$$

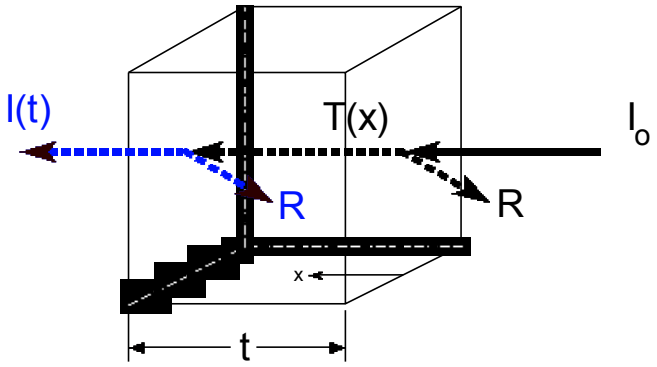

Figure 5: Sketch of light transmission through an object.

The transmittance T_λ is the ratio of the light transmitted versus the incident light intensity according to the Beer- Lambert law:

$$T = (1-R)^2 e^{-\alpha x} \qquad (4)$$

A linear relation is established from equation (4):

$$\ln (T) = 2\ln (1-R) - \alpha x \qquad (5)$$

which shows ln (T) to change linearly with the plate thickness, and the change rate equals $-\alpha$. α is the absorption coefficient which depends on the absorber chemical composition and the light wavelength, and x is the path length (i.e., plate thickness for lithophanes).

This equation shows that the transmittance decreases exponentially with increasing path length. A portion of the transmitted light is internally reflected as it exits the material. A portion continues to reflect internally each time it interacts with one of the two surfaces. The total light transmitted then may be written as:

$$T = \sum_{n=1}^{\infty} (1 - R)^2 e^{-\alpha x} \ (1 + R^{2n} e^{-2n\alpha x}) \qquad (6)$$

Applying a Taylor's series expansion,

$$T = \frac{(1-R)^2 e^{-\alpha x}}{1-R^2 e^{-2\alpha x}} \qquad (7)$$

For a given absorption coefficient and refractive index, transmittance can be solved using this modified Beer-Lambert Law.

1.4.2 Introduction of Molecular Electronic Transition

Molecular electronic transition takes place when electrons in a molecule are excited from one energy level to a higher energy level. The energy change associated with this transition provides information on the structure of a molecule and determines several molecular properties such as the color (Molecular electronic transition, 2011). The electronic transitions in organic compounds can be determined by ultraviolet-visible spectrosocopy, provided that transitions in the ultraviolet (UV) or visible range of the electromagnetic spectrum exist for this compound (Morrill *et al*, 1981; Crouch and Skoog, 2007).

There are four energy levels in the hypothetical electron energy theory: sigma- pi-n- pi*- sigma*, in which order the energy increases. The sigma and pi levels are bonded, the n level is nonbonding level, and pi* and sigma* are antibonding levels (Chem, 2009). The electron transitions mentioned in this work are: pi-pi* transition and n-pi* transition. The pi-pi* transition means the electrons occupying a pi-bonding orbital can get excited to the to an anti-bonding pi orbital*. And the n-pi* transition corresponds to the n to pi* orbital electron transition.

1.4.3 Investigation of Polymer Film Transmittance

Studies have been performed to investigate the transmittance of several polymer based films (Tang and Liu, 2008; Bak *et al*., 2010; Sung *et al*., 1994; Liu *et al*., 2012; Xue *et al*., 2010; Lai *et al*., 2009). Tang *et al*. (2008) found that pure PVA (poly(vinyl alcohol)) films have constant higher transmittance (85-90%) than 2%-60% CNM (cellulose nanofibrous materials) reinforced PVA (45-80% transmittance) or CNM films (10% transmittance) in the 350-800 wavelength range. Also, the transmittance increased with increasing wavelength from 350-450 nm but then remained constant.

Bak *et al*. fabricated electrically conductive transparent films from SWNT (single-walled carbon nanotubes) and electrospun nylon 6 membranes. They measured the transmittance with an Agilent 8453 UV-visible spectrophotometer (Agilent Technologies, Germany) from 380-750 nm. High transmittances were obtained in 0.01-0.03 wt% SWCNT films especially for 0.01-wt% SWCNT film (80- 90%), which slowly increased with the wavelength from 350-750 nm.

Sung *et al*. (1994) showed a plot of UV-visible spectra of PPy-N (polypyrrole-nylon 6) composite films with different reaction times (5 min, 30min, 2h and 4h) and identical diffusion and reaction temperatures (20 °C). They found that a shorter polymerization time resulted in a higher transmittance due to the absorption band from the π- π^* transition (Street *et al*., 1982).

1.4.4 Investigation on Reflection and Absorbance

Direct measurement of powder transmittance is difficult and inconvenient due to its loose form. Instead, research has consisted of acquiring powder absorbance and using Eq. (2) to obtain powder transmittance. Liu *et al*. (2008) pointed out the reflection could be ignored when the powder particle diameter is lower than 400 nm since visible light may theoretically pass particles without the occurrence of reflection/refraction since at the interface light is an electromagnetic wave.

Tolochko *et al*. (2000) published the normal spectral absorbance of several metal, ceramic and polymer powders that are usable for laser sintering using an integrating sphere with two different lasers: Nd-YAG (λ=1.06μm) and CO_2 (λ=10.6μm). An integrating sphere is a hollow spherical cavity whose interior is covered by a diffuse white reflective coating (Greenham *et al*., 1995). It obtains the reflectivity by taking the ratio of reflected light intensity to the incident light intensity. It is found that metal and carbide absorbance decreases with increasing wavelength, while oxide and polymers behave the opposite way. The powder mixture absorbance is proportional to the component absorbance and the component volume fraction.

Sung *et al*. (1997) measured the absorbance of polyaniline-nylon 6 composite film with a UNICAM 8700 series spectrophotometer, finding for HCI-doped PANI (polyaniline), the absorption band at 345 nm is a π- π* transition. The absorbance at 400 and 815 nm arise from the polaron transitions with absorption bands for PANI-N (polyaniline-nylon 6) appearing at 360, 420 and 840 nm, respectively.

1.5 BRIGHTNESS, GRAYSCALE AND CONTRAST

1.5.1 Concepts and Illustrations

A grayscale digital image is an image in which the value of each pixel is a single sample, which means it carries only intensity information (Johnson, 2006). Grayscale levels in black-and-white digital images are commonly stored with 8 bits per pixel, which allows 256 shades or levels of gray. These levels of gray generally vary between 0 (black) and 255 (white) as shown in Figure 6 below.

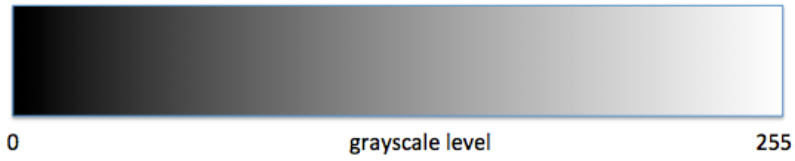

Figure 6: Illustration of grayscale level versus black and white color.

Brightness is a visual feature which may be described as the average grayscale level of an image. Bright images have large average grayscale levels while dark images have low grayscale levels. In software, an image may be made brighter or darker by either adding or subtracting a constant number of grayscales to every pixel as shown in Figure 7 below. Since the range of grayscales is 0-255, the image will tend to wash out if large numbers of pixels are changed to become either 255 (white washout) or 0 (black washout).

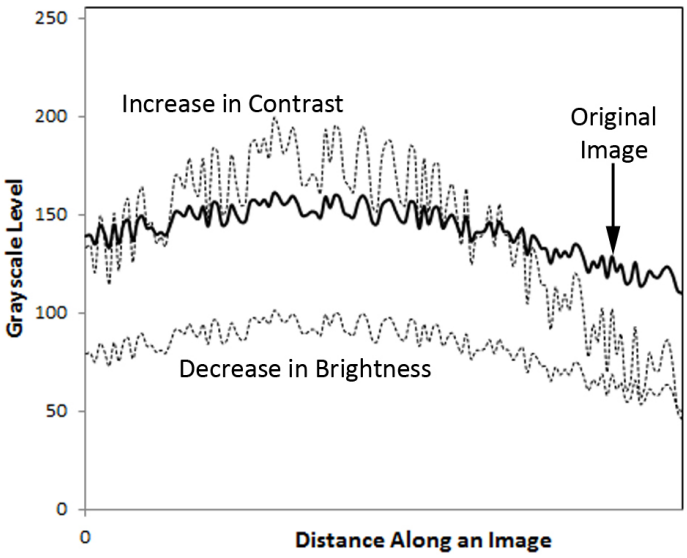

Figure 7: Schematic pixel line of an image illustrating the change in grayscale level associated with an increase in contrast and a decrease in brightness.

Contrast is an indication of the change in luminescence of an image relative to its surroundings. There are several methods for quantifying the contrast. The contrast of an image may be changed by multiplying each pixel's grayscale deviation from the average value by a number less than one (decreasing contrast) or greater than one (increasing contrast). Decreasing contrast transforms an image in the extreme to a uniform grayscale equal to the average grayscale level. Increasing contrast in the extreme produces an image for which each pixel's grayscale level is either 0 or 255 depending on whether the original pixel grayscale level was less than or greater than the average grayscale level, respectively.

1.5.2 Quantification of Brightness and Contrast

Brightness and contrast may be quantified. Suppose an image has an average grayscale level G_{ave}. The brightness and contrast of a pixel may be changed according to the following relation:

$$G = G_{ave} + B + f*(G - G_{ave}) \qquad (8)$$

where G is the adjusted grayscale level, B is change in grayscale associated with brightness and f is the change in grayscale associated with contrast, appreciating that the minimum possible value of G is zero and the maximum possible value of G is 255. Large values of B and f result in bright and high-contrast adjustments, respectively.

1.6 ADDITIVE MANUFACTURED OPTICAL PARTS

1.6.1 ASTM Standard Terminology for AM

ISO/ASTM 52921: 2013 (E) (2013) established the standard coordinate systems and test methodologies for additive manufacturing processes. The build platform, build surface and orthogonal orientation notation will be introduced here.

A. AM machine coordinate system

The build platform is any base that provides a surface upon which the build is started and supported throughout the build process (see Figure 8). In some systems, parts are built attached to the build platform, either directly or through a support structure. In powder bed systems, no direct mechanical fixture between the build and the platform may be required.

Build surface is the area where material is added, normally on the last deposited layer which becomes the foundation upon which the next layer is formed.

The front of the machine is designated by the machine builder. Generally this is the side of the machine that the operator faces to access the user interface or primary viewing window, or both.

The machine coordinate system is a three-dimensional Cartesian coordinate system as defined by a fixed point on the build platform with the three principal axes labeled X, Y, Z. The origin is a designated reference point at which the three primary axes in a Cartesian coordinate system intersect, which is the zero point, or (0,0,0) when using XYZ coordinates.

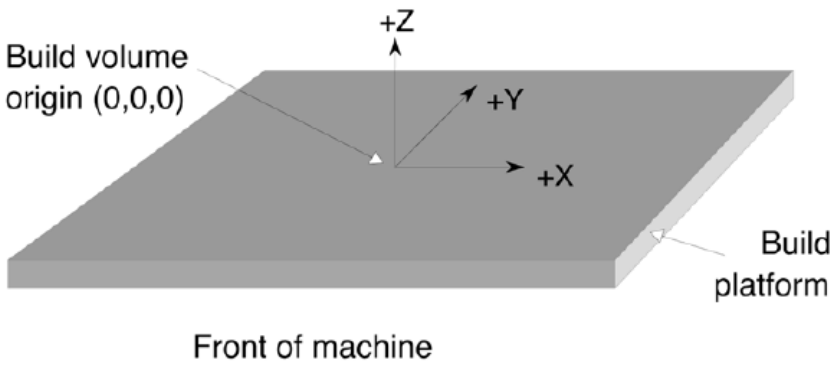

Figure 8: Generic (upwarding building) AM system. From ASTM 52921.

B. Location and orientation of parts within the build volume

The arbitrary oriented minimum bounding box is the minimum perimeter cuboid that can span the maximum extents of the points on the surface of a 3D part calculated without any constrains on the resulting orientation of the box as seen in Figure 9.

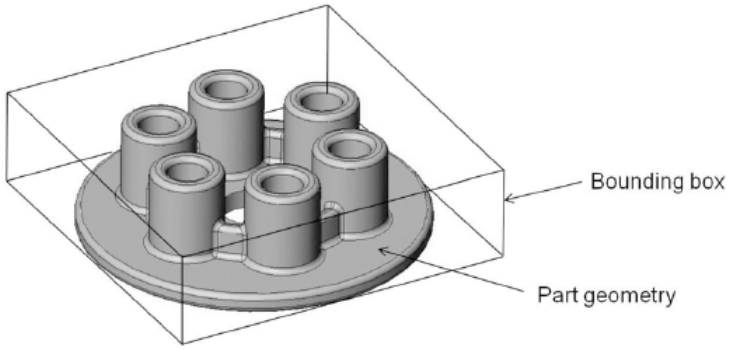

Figure 9: Example of an arbitrarily oriented minimum bounding box.

The orthogonal orientation notation is the part initial build orientation and may be used when the intended build orientation for a part is such that its arbitrarily oriented minimum bounding box is aligned parallel to the X, Y, and Z axes of the build volume.

Its orientation may be described by listing which axis is parallel to the longest oval dimension of the bounding box first, followed by the axis which is parallel to the second longest overall dimension of the bounding box second, followed by the axis which is parallel to the third longest overall dimension of the bounding box. For example, a specimen which is placed so that its longest dimension is parallel to the X axis, the second longest dimension is parallel to the Y axis, and its shortest overall dimension is parallel to the Z axis shall be defined as having a XYZ orientation as shown in Figure 10 below.

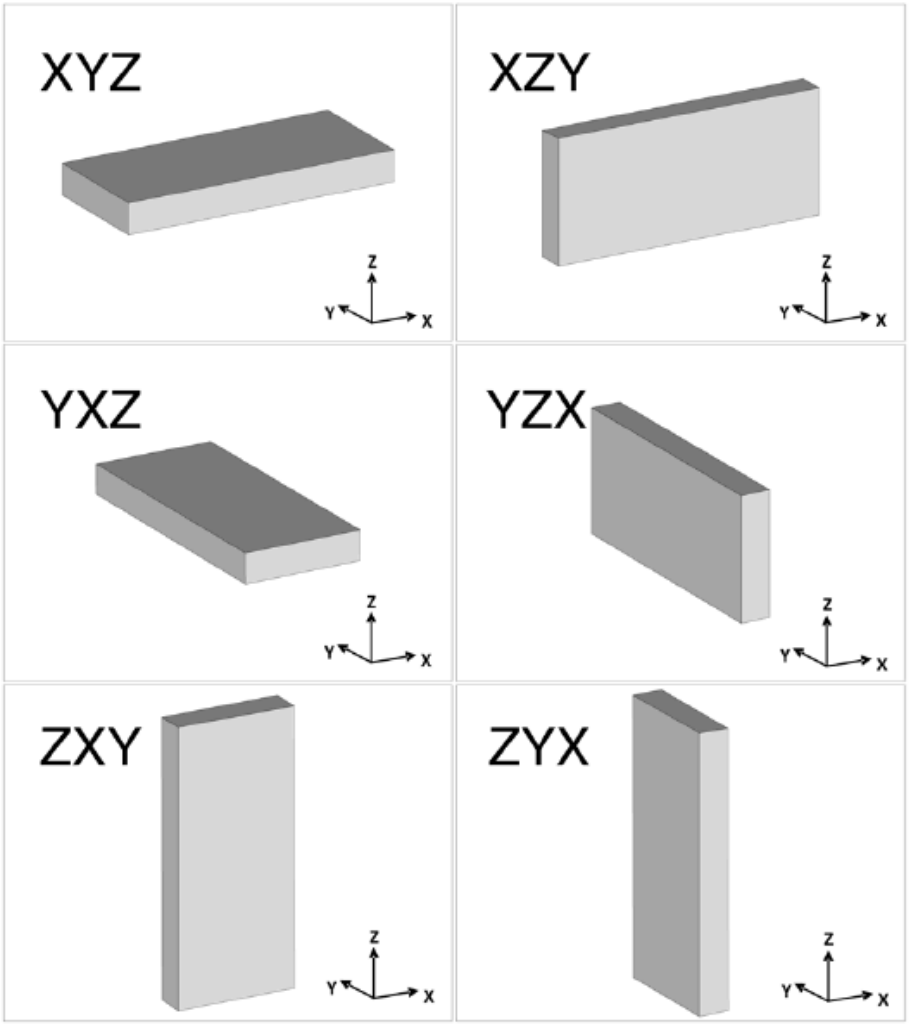

Figure 10: Orthogonal orientation notation, per ISO/ASTM 52921: 2013 (E).

1.6.2 Manufacturing orientation effects on LS

Basically, there were two building orientations during LS process: 'flat' build in the XY plane, or 'stand' build on the edge in the ZX/ZY plane. 'Stand' manufacturing orientation results in better lithophane surface quality and enlarged contrast but causes much more time and material. 'Flat' building leads to less lithophane contrast due to the layer limitation, but causes less time and material.

For example, if build a 100 by 25 by 5 mm lithophane in the XY plane, the height of the build would be 20 mm; while build in the Z plane, the build height would be 40 mm. This means if the product quantity is low, building in the XY plane is a better option; if a large quantity is needed, building in the Z plane would be better. The detailed discussion is presented in Section 4.5.4.

1.6.3 Other AM Technologies

The predominance of AM literature dealing with optical properties centers on transparency. Stereolithography (SL) has for some time had commercial transparent materials available. Other processes such as Rapid Freeze Prototyping are naturally amenable to production of transparent parts in ice (Zhang *et al*, 1998). The issue with other AM technologies including ink-jet printing, laser sintering and fused deposition modeling, is avoiding internal reflections from surfaces which impede transparency.

Niino at The University of Tokyo was among the first to explore use of refractive index matched infiltrants to produce transparent laser sintered parts (Niino, *et al*., 2004; Niino and Yamada, 2005). Suwanprateeb and Suwanpreuk produced transparent ink-jet printed parts by mixing polymethyl methacrylate powders with maltodextrin binders followed by infiltration with a heat-curing acrylic (Suwanprateeb and Suwanpreuk, 2009).

1.6.4 Motivation

Several topics are investigated in this chapter: laser sintering history, SinterStation introduction, SinterStation parameters; common LS materials including metal, ceramic and polymer; background and literature review for lithophanes; light transmission concepts and relevant calculations when light passes through a object, investigation of polymer film transmittance, reflection, and absorbance; the concept and quantification of image brightness and contrast, ASTM part orientation standard and other AM technologies producing translucent polymer parts are included.

Since no systematic study on laser sintered polyamide 12 optical properties or manufacturing issues was conducted before, this work is considered to be the first effort to analyze the optical properties and additive manufacturing of laser sintered polyamide 12 translucent parts, which are essential for lithophane application. Lithophanes made with other AM processes (i.e., stereolithography) were studied as a comparison to the LS process and other laser sinterable materials were investigated.

Chapter 2: Methods

Six sections are included in this chapter. First, the LS material is selected; second, the SinterStation setup is discussed. The method for grayscale to thickness conversion is described. Evaluation specimens and lithophane build preparations are described. Third, light transmission experiments are detailed, including the operation of the spectrophotometer, light meter and light table. Fourth, wavelength dependence experiments are described including the light source, lithophanes and stair-stepped plate fabrication. Fifth is the stereomicroscopy. The last section deals with surface finish experiments, with experimental design, surface preparation by polishing, and light transmission experiments included.

2.1 LS Material

According to Eq. (2) and (3), high transmittance is obtained with small n (refractive index). Comparing ABS, PLA, PVA, PA 12, PMMA and HDPE densities, refractive indexes, melting points, prices, and mechanical properties (Tang *et al*., 2008; Tang *et al*., 2011; Zhang *et al*., 2009; Rhim *et al*., 2009; Hughes *et al*., 2012), PA 12 was chosen as the experiment material.

PA 650 produced by ALM® was used in laser sintering. Detailed mechanical and thermal properties are shown in Table 3 below (ALM PA 650 Technical Data Sheet, 2011). Its reported average particle size is 55 μm, and the powder feedstock was a sifted mixture of equal parts of fresh powder, part cake and feed bin powder. Mixing was performed using an IMER mixer with a mixing time of 1hr at 23 RPM.

Property	Test Method ASTM	Unit	Value
Bulk Density	D1895	g/cm^3	0.46
Sintered Part Density	D792	g/cm^3	1.02
Ultimate Tensile Strength	D638	MPa	48
Tensile Modulus (XY)	D638	MPa	1700
Flexural Modulus (XY)	D790	MPa	1500
Elongation properties (XY)	D638	%	24
Crystalline melting point	D3418	ºC	181

Table 3: Mechanical and thermal properties of polyamide 12 powder. From ALM PA 650 Technical Data Sheet (2011).

At room temperature, the refractive index for polyamide 12 is 1.53 (Springer, 2005), substituting into Equation 3, R = 0.04454. Equation 2, 5 and 7 can be rewritten as:

$$A + T = 0.95546 \quad (9)$$

$$\ln (T) = -0.091 - \alpha x \quad (10)$$

$$T = \frac{0.9129e^{-\alpha x}}{1-0.0020e^{-2\alpha x}} \quad (11)$$

2.2 LASER SINTERING

2.2.1 SinterStation

A. Process

The first step in LS was to load PA 12 powder into the feed bins. The part bin was filled with a thin layer of powder typically less than 12 mm, to insulate the top of the part piston. The build chamber was preheated to a temperature that varies depending on which machine is used, measured at the powder surfaces, and held for a time to allow the walls to approach thermal equilibrium.

After the preheat period, several layers of powder were deposited and heated to the operating temperature. The build began, with CO_2 laser beam scanning the pre-designed pattern into the heated powder. (Tim *et al*., 2013). The laser worked repeatedly on the direction parallel to X- axis first, then scanned parallel to the Y-axis on the next layer.

After the pattern had been scanned in a layer, a new layer of powder with 0.075 or 0.1 mm thick was deposited and heated. In this way, the part was built up. A 200 mm by 150 mm by 0.254 mm thick heat shield was built before laser sintering the functional parts. This was done to prevent shrinkage during part manufacturing and part bed cooling.

After the last layer was finished, a cool-down stage (usually 2.54 mm in the SinterStaiton HiQ) took place in which several layers of powder were deposited to insulate the top of the part. The part was allowed to cool *in situ* before removal. Over-fast cooling leaded to unacceptable geometric distortion of the part.

B. Operating temperature evaluation

It is important to acquire proper operation temperatures on left/right feed bins and the part bed for the optimal LS performance. To obtain the most proper temperature for the feed bins, after reaching the initial warm-up set points on feed bins (around 50 °C), feed bins setup points were manually increased by 1- 2°C after every 2-3 layers of powder were added.

The maximum feed temperatures were reached when the feed bed started to show subtle cracking, or ripples were observed on the part bed surface. The proper feed heater setup points were 1 °C below the maximum feed temperature. Moreover, the setup points might be different on left and right feed bins, due to the individual heater performance and heat leakage on each side (Yuan *et al.*, 2012).

To evaluate the proper operating temperature for the part bed surface, careful observation of the heat shield part building was essential. First, the part bed temperature was set to a relatively low operating temperature, ~171°C. If slight curling was seen during a part build, the part bed setup point was increased by 2°C. The process was repeated until non-curling flat layers were obtained.

Laser scan powers on SinterStation 2500 and HiQ for thin layer thickness were obtained by building evaluation bars on the Sinterstation and observing the part quality. Evaluation bars were built with laser scan powers from 12 to 22 W with 2W separation.

The operating temperatures, warm-up and cool down heights, and laser scan powers varied between the different machines (SinterStation® 2500 and HiQ™) and are shown in Table 4 below.

Operating Parameters		SinterStation 2500	SinterStation HiQ
Warm-up Height (mm)		25.4	12.7
Left Feed Bin Operation Temperature (°C)		78	140
Right Feed Bin Operation Temperature (°C)		82	140
Part Bed Operation Temperature (°C)		170-173	173-174
Cool-down Height (mm)		12.7	2.54
Laser Scan Power (W)	0.1016 mm layer thickness	3.6	1.5- 2.0
	0.0762 mm layer thickness	24- 30	15- 18

Table 4: Operation properties for SinterStation® 2500 and HiQ™ .

2.2.2 Grayscale to Thickness Conversion

The software utility, Bmp2Cnc, was used to convert the grayscale jpg/bmp digital photo to a three- dimensional CAD file. It is based on a relation that linearly translates each pixel grayscale level to a respective height. It reads the file in bitmap format, generally 8 bits. Z-axis depth is changeable based on the manufacturing requirements.

The basic operation steps were: first, the grayscaled image (bmp or jpg format) was generated into the software; second, the size of the model that would be manufactured was set up with roughly 150-200 mm in length. The width would be adjusted automatically based on the original image length/width ratio; third, define the maximum thickness for the lithophane, which spanned 2.54- 10.00 mm for this research work; last, the calculated file based on previous settings was generated, and saved as '.stl' with 'closed solid' format so a complete and closed graphic file was created.

2.2.3 Evaluation Specimens

A. Blank plate

All blank plates were manufactured on a DTM® SinterStation 2500 with 0.1016 mm layer thickness and 3.6 W laser scan power. Blank plates were built with dimensions 50.8 mm by 50.8 mm and with thicknesses of 0.38, 0.64, 0.83, 0.92, 1.30, 2.33, 4.74 mm, corresponding roughly to 4, 6, 8, 9, 13, 23 and 48 layers of powder during laser sintering with a layer thickness of 0.1016 mm. (System error of 5% on z-direction is included.) All blank plates were built in the XY plane in the build chamber.

B. Stair-stepped plates

Stair-stepped lithophanes were built with overall dimensions, 152.4 mm by 25.4 mm on the SinterStation HiQ with 0.1016 mm layer thickness and 25 W laser scan power. Equally spaced stair height ranged from 0.15 mm to 5 mm, with 0.97 mm height difference between each stair. Non-equally spaced stair heights were: 0.15, 0.56, 0.82, 0.99, 2.34, and 5 mm. All stair-stepped plates were built in the XY plane in the build chamber with 0.1016 mm LS layer thickness.

C. Plates with small features

All plates containing small features were built with overall dimensions, 25.4 mm by 12.7 mm by 5.08 mm plate thickness on the SinterStation HiQ with 0.1016 mm layer thickness and 25 W laser scan power. Two kinds of features were built on the 25.4 mm by 12.7 mm surface. One was cuboid, and the other was a semi-cylinder. On the plate with mini cuboids, the cuboids were 12.7 mm long, 0.254 mm thick with varying, equal-valued widths: 0.127, 0.254, 0.381, 0.508, 0.635, 0.762, 0.889, 1.016, and 1.524 mm. On the plate with semi-cylinders, the heights were 12.7 mm, and the diameters were the same as the values listed for the cuboid widths. All plates were drawn in SolidWorks.

Plates were enlarged linearly in all directions by a factor of three for better observation in Figure 11. Two plates placed on the back of the build were the ones mounted with semi- cylinders, one manufactured in the XZ plane and another one in the ZY plane. Two in the front of the build were the ones with cuboids. Tags were applied for distinction. The white sheet of paper shown in Figure 11 was the heat shield which prevents heat distortion after LS. The separation between the heat shield and plates was 2.54 mm.

The software used to set up the build was Build Setup version 3.42 from 3D Systems Incorporation®.

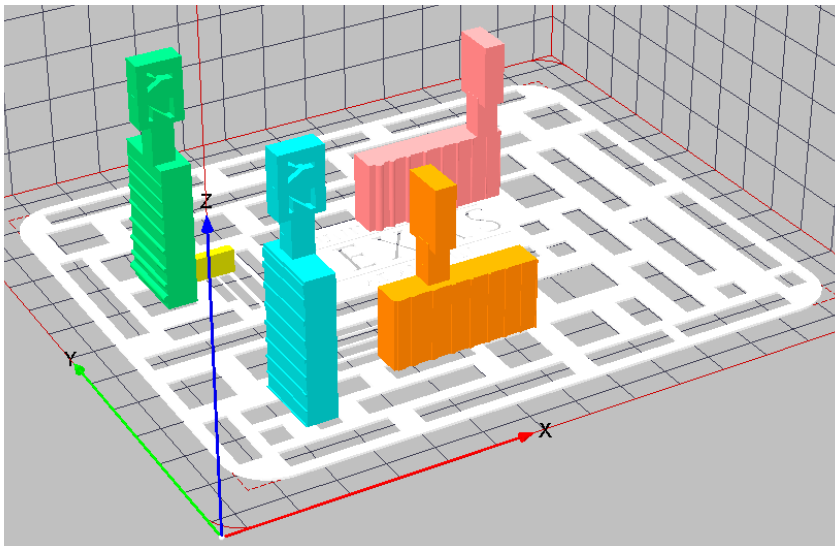

Figure 11: Build setup layout for plates with small features.

C. Wedge

Four wedges were built on the HiQ with 0.1016 mm layer thickness and 25 watts laser scan power, with dimensions of 101.6 by 25.4 by 10.16 mm. Part building orientations were shown in Figure 12 below. Two were built vertically, one with the bottom surface down, the other with the bottom surface up. The other two were built 'flat'. All wedges were marked with numbers for future reference.

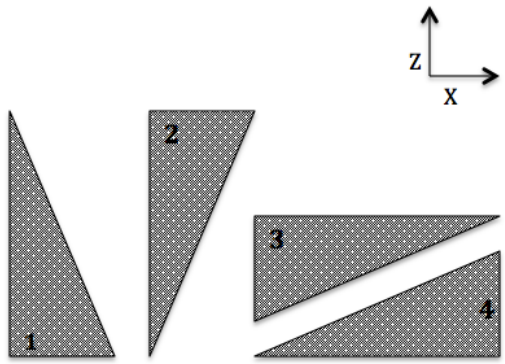

Figure 12: Schematic layout of the wedges in the build.

2.2.4 Lithophanes

A. Varying thickness

One lithophane was generated from Dr. David Bourell's digital image and built in the XY plane, with a dimension of 127 by 76 by 3.8 mm and sintered with layer thickness of 0.1016 mm. Other lithophanes were generated from a reproduction of Raphael's painting (Agnolo Doni). All lithophanes were used the software Bmp2Cnc, laser sintered on the DTM® SinterStation HiQ with basic operating temperature settings shown in Table 4. The lithophanes were built using different layer thickness, either 0.0762 mm (15 W laser power) or 0.1016 mm (24 W laser power).

There were two sizes of lithophanes: 127 mm by 76 mm, and 101.6 mm by 60.8 mm, with maximum plate thicknesses of 1.0, 3.0, 3.8, 5.0, 7.0 and 9.0 mm. To prevent the lithophane thinnest part from over melting, a thin sheet 0.2032 mm thick was attached at the bottom of the lithophane file, overlapping by 0.0508- 0.1016 mm to ensure two separate STL files would merge together when saved.

B. Varying building direction

To obtain the build orientation influence on lithophane surface quality, lithophanes with maximum thicknesses of 1.0, 3.0, 3.8 and 5.0 mm were first built in the XY plane and then built in the YZ plane and the ZX plane. Lithophanes with thickness of 7.0 and 9.0 mm were built in YZX plane. All parts were built with a 0.2032-mm sheet attached with an overlap distance of 0.0508- 0.1016 mm.

C. Performance comparison

Lithophanes were placed on a back lit light box (described in Section 2.3.2), with thicknesses increasing from left to right. Lithophanes sintered with the same layer thickness were laid in a row. Images were captured using a SONY DSC- W55 camera.

2.3 LIGHT TRANSMISSION

2.3.1 Optical Evaluation

A Unico 1200 110V/50Hz S-1201 spectrophotometer with 5 nm bandpass and 4 cell holders for 10 mm square cuvettes was used. The monochromator is a single beam with a grating system of 1200 lines per mm. Wavelength range was 325-1000 nm with an accuracy of ± 2nm. The photometric transmittance accuracy is ±1.0%, and the light source was a tungsten halogen lamp 6V/10W.

Fifteen minutes warm up time was needed for the instrument, and measurement was made from 400 nm to 800 nm in 20 nm increments for all seven blank plates. The spectrophotometer was calibrated before each experiment by inserting a black rectangular block into the cuvette holder and setting 0% transmittance.

2.3.2 Light box

A Picker 240050 X-ray view/ light box was used in this research work. Its electrical settings were 115 V, 1.2 A, and 60 Hz. The view area is 457.2 by 368.3 mm with a total dimension of 558.8 by 393.7 by 95.25 mm. The light box produced unadjustable visually uniform white light over the view area.

2.4 WAVELENGTH DEPENDENCE EXPERIMENT

2.4.1 Light Sources

Monochromatic LEDs were obtained from Mouser Electronics, Inc. These diffused standard LEDs have the same viewing angle of 30° with different wavelength and luminous intensities. Detailed LED information is in Table 5 below. An electric 40W/120V soft white bulb was used to detect the lithophane transmittance under normal indoor environment. A PROMASTER SB800 flash diffuser was used to spread the concentrated light.

Color	Blue	Green	Yellow	Red
Wavelength (nm)	465	525	589	640
Light intensity (Milli-candela)	2600	12000	33000	15000

Table 5: Monochromatic LED properties.

2.4.2 Light Meter

A Dr. Meter Digital Illuminance/ Light Meter LX1330B was applied to ensure the same LED light intensity. The screen has 3-1/2 digit 18mm LCD, with a range of 0.1-200/ 2,000/20,000/ 200,000 Lux. The accuracy reaches ± 3% in the range of 0-20,000 lux and sampling rate is 2-3 times per second.

2.4.3 Light Transmission Apparatus

A circuit was created to maintain the same LED luminous intensity by applying 13.8V DC power and an OHMITE CU-1531 type AB adjustable resistor (0-15 kΩ). The power supply was a PYRAMID regulated PS- 9 KX model, with an input of 115V, 60 Hz, 70 W and output 13.8 V DC. A constant resistance of 550Ω was also used to prevent the LEDs from burning out. The circuit diagram is shown in Figure 13 below.

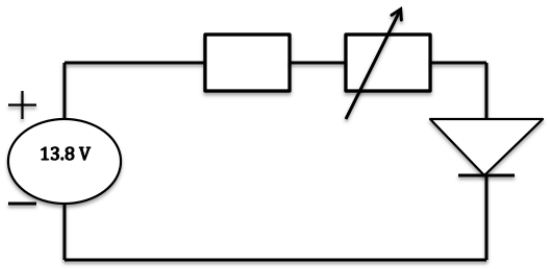

Figure 13: Electrical circuit diagram for LED power input.

Two kinds of experimental specimens were used. First was a lithophane built in the XYZ plane with maximum thickness of 3.81 mm. The second was the stair- stepped plates described in Section 2.2.3, including the evenly stepped and unevenly stepped plates.

For monochromatic light transmittance of lithophanes, a light source and measurement apparatus were constructed, Figure 14. The locations of the light source, light meter and camera were constant for maintaining image-capturing consistency. A PROMASTER SB800 flash diffuser was used to spread the concentrated light. The distance between the diffuser and the light meter was constant at 25 mm, and the distance between the diffuser and the test specimen was 80 mm. Photos were captured by the SONY DSC- W55 camera at a distance of 150 mm away from the lithophane.

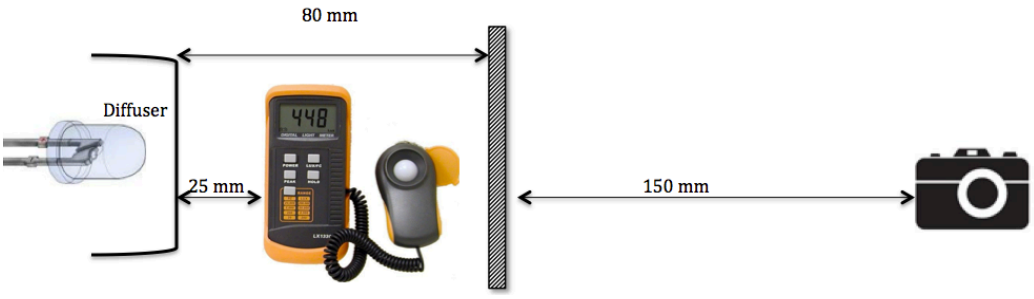

Figure 14: Experiment layout for lithophane image capturing.

2.5 STEREOMICROSCOPY

2.5.1 Stereomicroscope

A Nikon SMZ 1500 stereomicroscope was used in this work, with two plastic Nikon 150W high intensity fiber optic episcopic illuminators that providing lights from left and right sides onto the specimen. The magnification was adjustable between 0.75 and 11.25. Nikon- 150 illuminators had 21V, 150 W lamps with a voltage of 230 VAC at 50/60 Hz. The intensity control was 0-100% with the noise level less than 24dB.

In this research work, the top light source was used with an intensity of 50% (75W). The magnification was 0.75X- 1.0X. A piece of metal and soft black clay was applied to stabilize the specimens on the stage and also provided a dark background.

2.5.2 Specimens

A. Lithophanes

Lithophanes with thickness of 3.00 mm built in the XY and YZ planes were viewed through the stereomicroscope to assess the nature of layering. On the reproduction of 'Agnolo Doni' shown in Figure 15, the clouds on the right side in the middle of the lithophane (highlighted with a black lined triangle) and the ties in the center of the figure (highlighted with a white rectangle) were observed under 1.5x magnification.

Figure 15: Highlights of stereomicroscope examined areas on the painting reproduction.

B. Wedge

A piece of black paper was placed on the stereoscope platform to enhance image contrast. Photos were taken on the thin flat part of the wedge and the sharp ends. Comparisons were made between each of the four samples. The magnification was 1x.

C. Plate with small features

A piece of black paper was placed on the stereoscope platform to improve image contrast. Photos were taken on the plate sides to capture the cuboid and semi-cylinder shapes. Comparisons were made between each of the four samples. The magnification was 10x.

2.6 SURFACE FINISH EXPERIMENTS

2.6.1 Surface Finish Experimental Design

To analyze the effect of surface finish on the lithophane performance, five blank plates were built with dimensions, 50.8 by 50.8 by 12.7 mm. The polishing experiment was conducted at Harvest Technologies, Belton, Texas. Lithophanes were first infiltrated with cyanoacrylate to obtain a brittle surface to polish, since the polymer tended to deform and create strands or scratches when sanded. Further, the superglue would soak into any surface porosity of the part, which induced the possibility of changing the part transmittance.

An initial experiment was designed to analyze the cyanoacrylate effect on the laser sintered PA 12 transmittance. A piece of the specimen was infiltrated on one surface, and a second piece was infiltrated on both surfaces. To investigate the polishing effect, a third piece was infiltrated and polished on one side, while a fourth piece was infiltrated and polished on two sides. The fifth piece was neither infiltrated nor polished as a comparison specimen.

The second experiment was to examine and compare the optical transmittance change of all four post-processed plates and the non post-processed plate under spectrophotometer with varied monochromatic wavelengths. Also the thickness was measured and considered as a factor that affected the plate transmittances.

The last experiment was conducted to learn the polishing effect by comparing the non post-processed plate, both surface polished plate, and one surface polished plate performances on the white light box. Photos were taken first with the one surface polished plate polished surface on top, then polished surface on bottom, both accompanied with the non post-processed plate and both surface polished plate on two sides.

2.6.2 Surface Preparation by Polishing

The superglue brand was LOCTITE® 406 Prism Instant Adhesive which mainly is cyanoacrylate. A fast tack called Sprayway® 092 was used to accelerate the bonding. Regular 180 μm sandpaper was used to polish the surface, and a mechanical sanding device-orbit sander was used for auto-polishing.

First, an air blaster was used to remove dust and powders on the sample. Cyanoacrylate was spread evenly over the surface so it soaked into the porosity of the part. Fast tack was then applied on the sticky surface before it was completely dry. A few drops of fast tack was needed since too much would cause bubbling on the surface. The surface was cleaned using a bead blaster to accelerate the drying process and remove the residual glue. Once coated and dried, 80 μm grit paper was sometimes manually applied if the surface was very rough. 180 μm grit paper was used manually to remove the uneven glue. Then the orbit sander with grit size of 240 μm was used as the last polishing step.

2.6.3 Surface Roughness Experiment

Mitutoyo SJ-201 digital stylus profilometer was used to test the surface roughness. The measuring force range was 0.75- 4 mN, and cutoff lengths were 0.254, 0.762, and 2.54 mm, corresponding to different Ra ranges: 0.02- 0.10, 0.10- 2.00, and 2.0- 10.03 mm. Each sample surface roughness was examined, the average value and standard deviation of Ra, Rq, and Rz versus the non post-processed surface, cyanoacrylate infiltrated surface, and polished surface were plotted. The cutoff length for the non post-processed plate was 2.54 mm, and the cutoff length for cyanoacrylate infiltrated plate and polished plate was 0.254 mm.

2.6.4 Light Transmission Experiments

For light transmission measurement, first, thicknesses were measured on each polished sample. Light transmission experiments were conducted on all five specimens using the Unico 1200 110V/50Hz S-1201 spectrophotometer under wavelengths of 460, 540, 580, and 640 nm, which were typical wavelengths for monochromatic blue, green, yellow, and red lights. The transmittances for each plate were recorded and plotted versus wavelengths. Results were compared with each other.

Three specimens were placed on the light table for comparison: the non-polished, non- cyanoacrylate infiltrated standard, one specimen with one face polished, and one specimen with both faces polished. Photos were first taken with the one-face polished specimen polished surface on top, and then retaken with the specimen polished surface on bottom.

Chapter 3: Results

Five sections were included in Chapter 3. First, optical properties of laser sintered polyamide 12 blanks were investigated. Second, laser sintered polyamide 12 lithophanes were manufactured with varying plate thickness and layer thickness in the XY plane. The proper thickness correction was quantized for lithophane optimal performance, and error analysis on layer thickness adjustment was conducted.

Third, surface finish experiments were conducted. Fourth, the lithophane performance with different light orientation was presented. Finally, there was a study of lithophane manufacturing orientation.

3.1 OPTICAL PROPERTIES

3.1.1 Light Transmission

The effect of the wavelength on laser sintered polyamide 12 transmittance is shown in Figure 16. Plate thickness ranged from 0.38 to 4.74 mm. Wavelength changed from 400 to 800 nm with 20 nm separations. Twenty-one measurements were made for each plate. The range of transmittance was 10% to 88%. Transmittance first increased linearly from 400 nm to the peak of 540 nm (25-87%) and dropped to a minimum at 580 nm. It then remained almost constant from 600 nm to 800 nm. At a constant wavelength, transmittance decreased monotonically with increasing plate thickness.

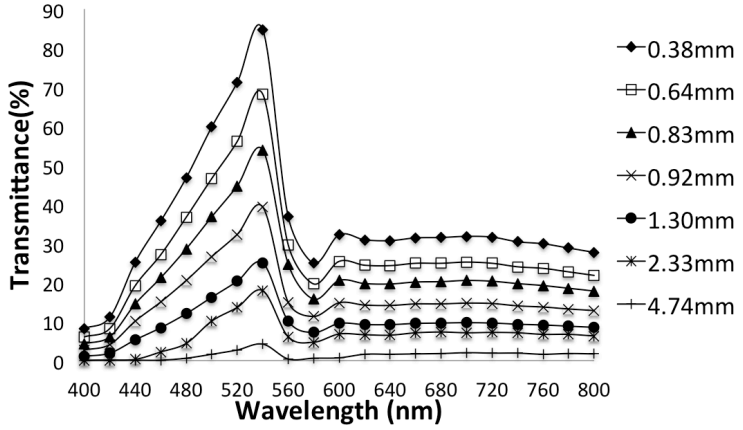

Figure 16: Effect of spectrophotometer wavelength on transmittance of laser sintered polyamide 12 plates with different thicknesses.

The influence of plate thickness on laser sintered polyamide 12 transmittance is shown in Figure 17 below. Seven measurements were taken and averaged for each monochromatic light scattering. The transmittance of PA 12 plates with a common soft white bulb is presented as well.

The white light effect was also calculated based on the theory that white light is a combination of all lights and there is no clear boundary between one color to another (Bruno and Svoronos, 2005). The estimate was obtained by averaging of transmittances of the red, green and blue LEDs, which are the three primary colors. The calculation results matched well with the soft white bulb experimental results, except that the transmittance of the 0.6 mm plate for the soft white bulb was 10% higher than the averaged result.

All plots show that transmittance decreased with increasing plate thickness. A sharp transmittance reduction was found at around 0.8 mm plate thickness. Green light had the highest transmittance, showing the largest sensitivity to thickness from 85% to 20% with increasing plate thickness; the soft white bulb transmitted 20% less light compared to the green light, followed by blue, red and yellow light.

Calculation results were obtained from the modified Beer-Lambert Equation, Equation 10, with the absorption coefficient described and calculated in Section 3.1.2 B. The absorption coefficient for white light was the averaged value of absorption coefficient from monochromatic red, blue and green lights. All calculated results matched well with experimental data. The calculated results for green light were roughly 10% higher on thin plates, and 10% lower than experimental results on thick plates. The calculated results for blue, red, and yellow lights are 3-5% lower than the experimental data.

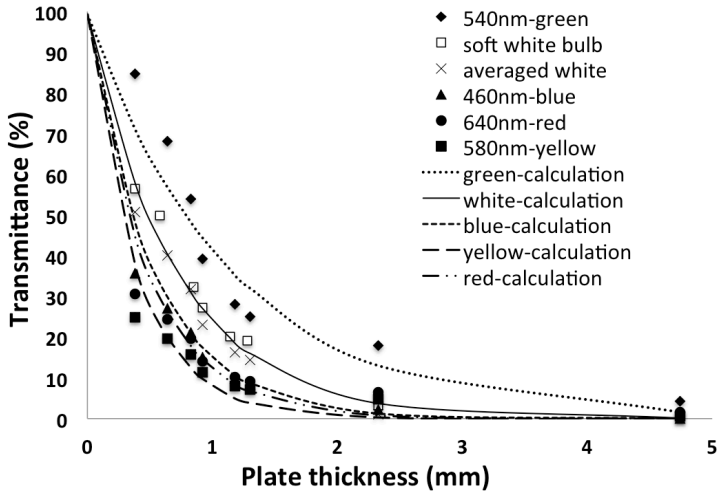

Figure 17: Effect of laser sintered polyamide 12 plate thickness on transmittance under different monochromatic lights and white light. Also included is a calculated dependence for white light based averaging red, green, and blue measurements. All calculated curves are based on Equation 10 with absorption coefficients obtained from the experimental measurements. The transmittances of melted LS blank (1.03 mm thick) were measured and fitted well with the calculation results.

3.1.2 Light Absorption

A. Absorbance

Laser sintered polyamide 12 blank plate absorbance results were obtained from Equation 9. Figure 18 shows the absorbance α at four plate thicknesses: 0.38, 0.83, 1.30, and 4.74 mm, respectively. The absorbance is reasonably the inverse of the transmittance. It was 95- 100% for 4.74-mm-thickness plate, and the minimum absorbance was 10% at 540 nm wavelength, for 0.38-mm-thickness plate. All trends started at around 90% absorbance for 400 nm wavelength, dropping to a minimum at 540 nm (monochromatic green light), with 95%, 73%, 45%, 10% absorbance, reaching a relatively high absorbance at 580 nm (monochromatic yellow light) with 95%, 90%, 80%, and 70%, then remained almost constant from 600 to 800 nm.

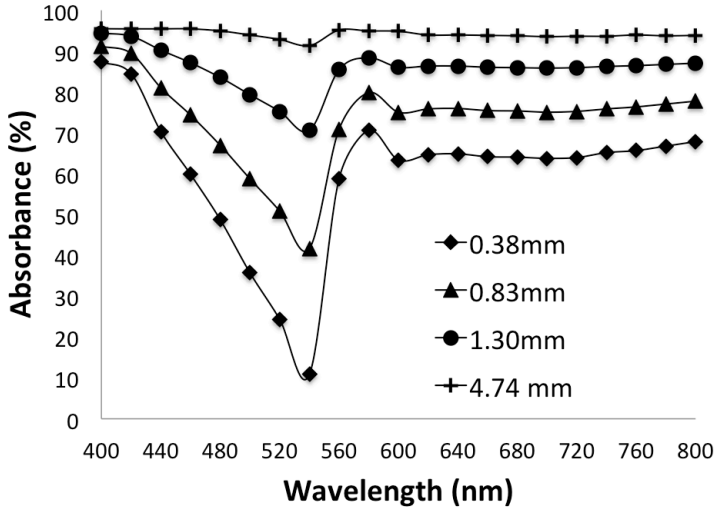

Figure 18: Effect of wavelength on absorbance of laser sintered polyamide 12 plates with four different thicknesses.

B. Absorption coefficient

The ln (T) was plotted against plate thickness in Figure 19 for four monochromatic colors red, yellow, blue and green. It showed with maximum plate thickness increasing, the ln (T) for green light decreased most slowly, followed by that for red, yellow, and blue lights. All plots changed rapidly with the maximum plate thickness range from 0.3 to 1.3 mm; then grew slower with 1.3 to 4.8 mm maximum plate thickness. The ln (T) for monochromatic blue light showed the most linearly decreasing among the four lights.

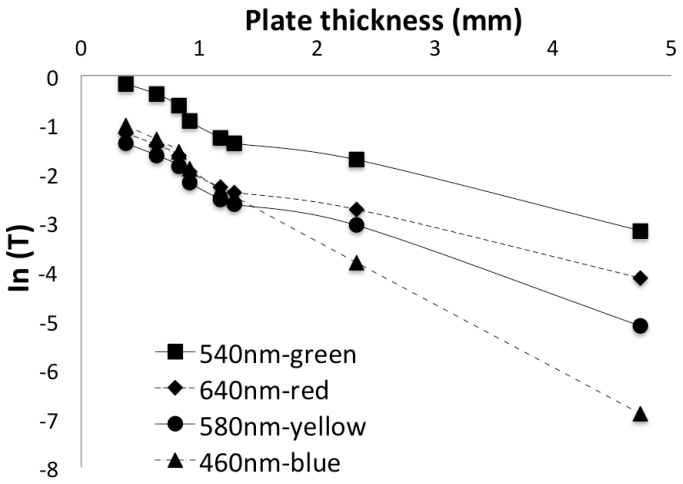

Figure 19: Plot of laser sintered polyamide12 blank plate natural logarithm of transmittance as a function of plate thickness under different monochromatic light: green, red, yellow and blue.

Based on Equation 10, the intercept was theoretically equal to -0.091 for polyamide 12 and applied for all colors in Figure 20. The intercept was forced to be the theoretical intercept, the linearized lines were fitted to the data, and the slope of the linearized plot was the negative of the absorption coefficient, which changed with transmitted light wavelength. It shows that the green light has the smallest absorption coefficient about 0.6 mm^{-1}, and the blue light has the largest absorption coefficient about 2 mm^{-1}, among the four monochromatic lights.

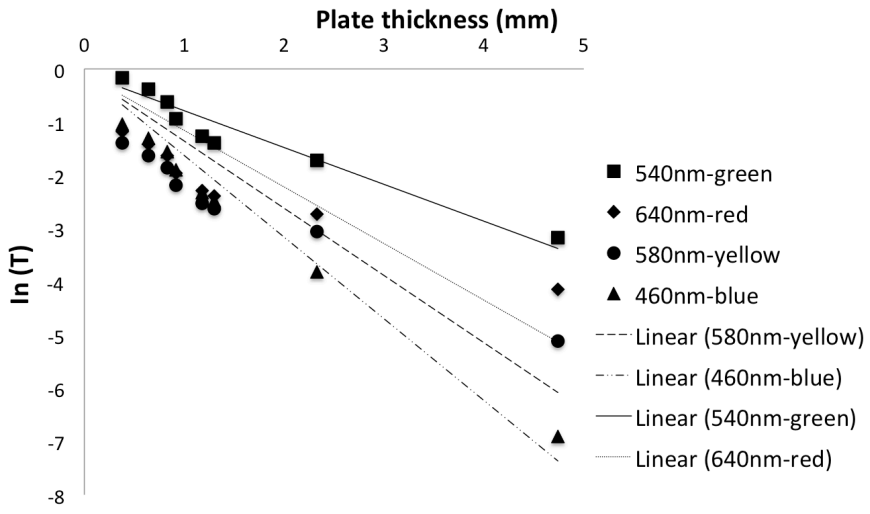

Figure 20: Linearized plot of laser sintered polyamide12 blank plate logarithm of transmittance as a function of plate thickness under different monochromatic light: green, red, yellow and blue, using the theoretical intercept of -0.091 based on a calculation using Equation 10.

Absorption coefficients were obtained as the slope of the linearized lines based on Figure 20. Figure 21 showed the relation between the absorption coefficients versus wavelength for polyamide 12 plates. The absorption coefficient decreases from 4 to 0.6 /mm in the wavelength range of 400 to 540 nm, increasing to around 2.5 /mm at 560-580 nm wavelength, then remaining almost constant. This trend was consistent with Figure 18, indicating that a larger absorption coefficient led to lower transmittance.

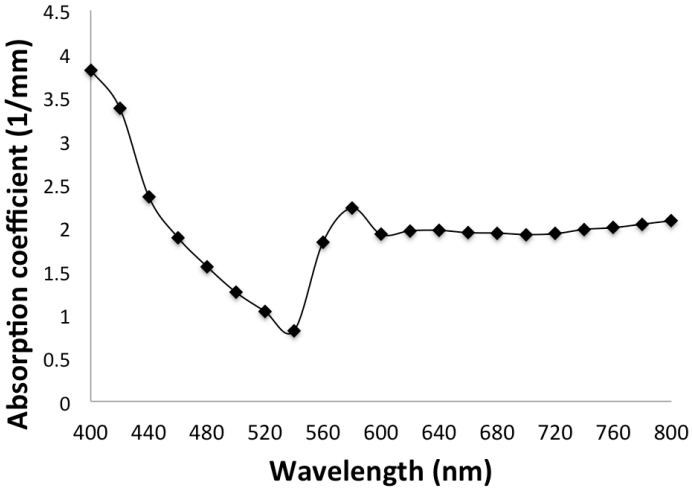

Figure 21: Plot of absorption coefficient versus transmitted light wavelength for laser sintered polyamide 12.

3.1.3 Wavelength Dependence Experiment

Figure 22 shows gray-scale photos of laser sintered PA 12 lithophanes under monochromatic transmitted light with the same light intensity, confirmed using a light meter. Lithophanes were built in the XY plane with 0.1016 mm layer thickness and 3.81 mm maximum plate thickness. The photo was a reproduction of Raphael's sketch, Agnolo Doni. It is clearly seen that the lithophane shows a larger contrast and better light transmittance under green transmitted light than under yellow light, which was consistent with the transmittance shown in Figure 16.

Figure 22: Gray-scale processed laser sintered polyamide 12 3.81 mm maximum thickness lithophanes under different monochromatic light: green (left), yellow (center). On the right was the initial digital image used to create the lithophanes.

3.2 LASER SINTERED LITHOPHANE MANUFACTURING

3.2.1 Quantized Thickness Correction in the XY Plane

The software used to convert the grayscale jpg digital photo to a three-dimensional CAD file was based on a relation that linearly converts the gray-scale level pixel to the height. However, according to Figure 17 and Equation 4, the relation between transmittance and thickness was not linear but rather varies with plate thickness. A correction had been made for transmittance under green light and white light, as shown in Figure 23. The relation that the conversion software used was shown by the dotted line on the figure. Both correction lines showed larger height value after original height beyond 1.3 mm, with a correction slope of 14.02 for green light and 7.93 for white light.

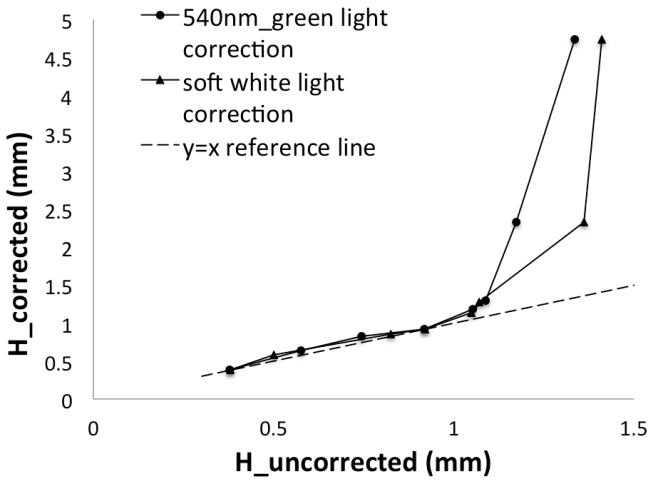

Figure 23: Correction relations between the original and updated heights on laser sintered polyamide 12 lithophane under monochromatic green light and soft white light.

Figure 24 illustrates this effect for two laser sintered stair-stepped lithophanes built in the XY plane with height ranging from 0.15mm to 5mm, one with constant height increment (bottom); another one (top) with varied height increment based on the monochromatic green light correction in Figure 23. Clearly, the corrected, upper sequence showed more uniform grayscale variation than the bottom sequence, which validated the need for a thickness correction. The effect of the correction is to make the darker pixels (lower grayscale levels) even darker.

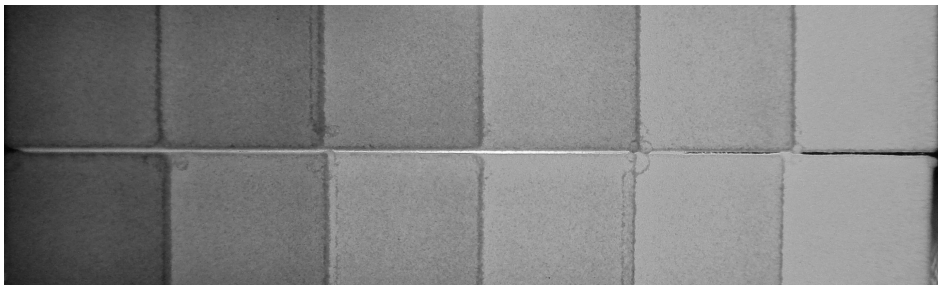

Figure 24: Grayscaled stair-stepped lithophanes. The height variation in the top sequence was based on monochromatic green light corrected values, whereas the bottom results were for constant changes in height. It was noted that the observed grayscale variation from light to dark is more uniform for the top, corrected sequence.

3.2.2 Layer Thickness

Figure 25 shows the figured lithophanes built in the XY plane, with the maximum plate thickness of 1, 3 and 5 mm from left to the right. The top sequence was built with layer thickness of 0. 076 mm and the bottom was built with layer thickness of 0. 1016 mm. The top group showed larger contrast compared to the bottom group. The top sequence lithophanes boundaries and features on the figure face, tie, and hands were more lucid compared to the bottom sequence. Also more contours were presented on the lithophanes built with 0.076 mm layer thickness.

(a)

(b)

Figure 25: Figured polyamide 12 lithophanes laser sintered with (a) 0.076 mm layer thickness; (b) 0.1016 mm of layer thickness. Maximum plate thicknesses of each group were 1, 3 and 5 mm from left to the right. Lithophane images were captured using a white light box.

3.2.4 Plate Thickness

Figure 25 illustrates lithophanes built in the XY plane with the same layer thickness (0.076 or 0.1016 mm) but different maximum plate thickness ranging between 1, 3, and 5 mm. The 1 mm thick lithophane showed the poorest contrast, while the 3 mm lithophane performed better, and the 5 mm lithophane performed the best. Comparing the figure jacket and hair, the 5-mm-thick lithophane showed the darkest features, while the 1-mm-thick lithophane showed the lightest with lowest contrast. Moreover, the 1 mm thick lithophane presented the greatest brightness on the background, followed by 3 and 5 mm lithophanes.

Figure 26 shows three lithophanes placed on a light box with photos captured through a digital camera. Figured lithophanes were built in the ZX plane, with layer thickness of 0.1016 mm and maximum plate thicknesses of 1,7 and 9 mm. The 1 mm thick lithophane showed the poorest contrast and largest brightness compared to 7 and 9 mm thick lithophanes. The 9 mm thick lithophane showed the best contrast since the four boundaries and the figure jacket were darker, and the features on the hands were more obvious. The 7 and 9 mm thick lithophanes also presented better contrast relative to the 3 and 5 mm thick lithophanes shown in Figure 25.

Figure 26: Figured polyamide 12 lithophanes laser sintered with 0.1016 mm of layer thickness built in the ZX plane. Maximum plate thicknesses were 1, 7 and 9 mm from left to the right. Lithophane images were captured on a white light box.

3.2.3 Error Analysis

Based on Figure 23, there was small range correction (less or around 0.1 mm) at the region where original height was less than 1.3 mm. However the SinterStation cannot delineate the corrected heights due to the manufacturing limit based on the available layer thickness. The difference between theoretical height and nearest actual height based on available LS layer thickness would reduce exponentially if the layer thickness were reduced from 0.1016 mm to 0.0762 mm. This is shown in Figure 27. The error per layer thickness reduced from 0.23 mm to 0.03 mm.

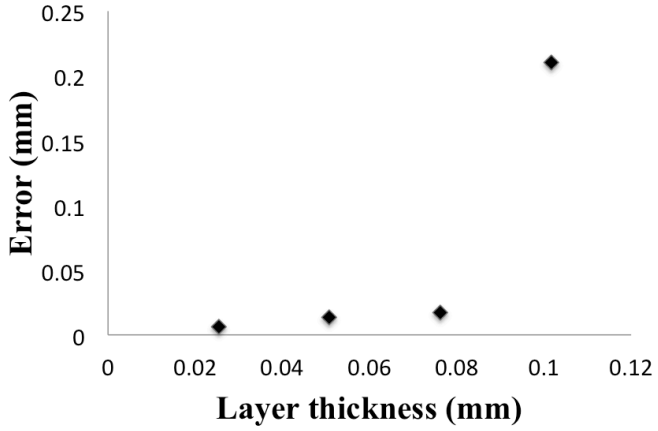

Figure 27: Error analysis on the difference between theoretical height and nearest actual height (0.64- 1.3 mm) based on available LS layer thickness versus layer thickness based on one layer for laser sintered polyamide 12.

Error analysis was also conducted for the original height range of 1.3 to 4.9 mm. This was shown in Figure 28. The difference between theoretical height and nearest actual height per layer based on available LS layer thickness was reduced linearly from 0.2104 to 0.0064 mm when the layer thickness decreased from 0.1016 mm to 0.0254 mm.

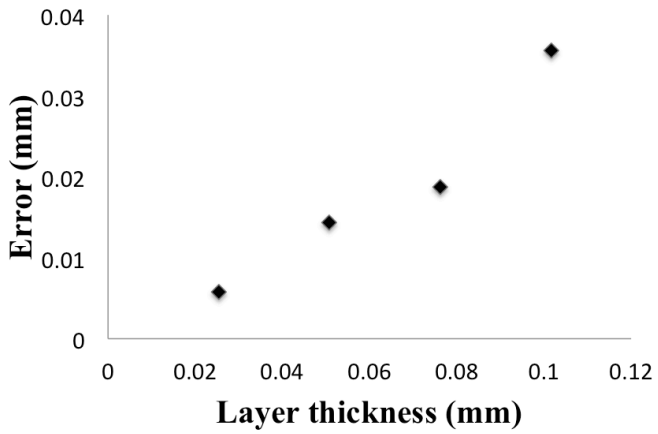

Figure 28: Error analysis on the difference between theoretical height and nearest actual height (1.3- 4.9 mm) based on available LS layer thickness versus layer thickness based on one layer for laser sintered polyamide 12.

3.3 SURFACE FINISH

3.3.1 Surface roughness experiments

Figure 9 shows the surface roughness results among the non post-processed, cyanoacrylate infiltrated, and polished surfaces. Each point was the average value of the surface roughness experimental mesurements. Error bar presented standard deviation is also shown. Surface roughness greatly decreased after the cyanoacrylate infiltration: Ra reduced from 90 to 25 μm; Rz and Rq decreased to around 5 μm. Then the surface roughness decreased to the minimum after the polishing, indicates the polishing process benefited the surface smoothness.

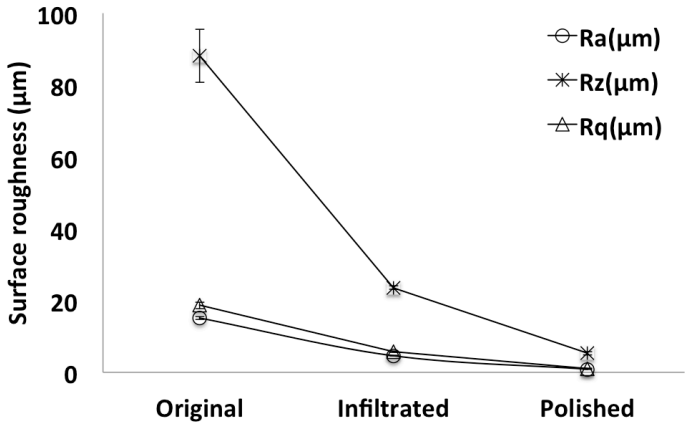

Figure 29: Surface roughness comparison among the non post-processed, cyanoacrylate infiltrated, and polished surfaces. Error bar presenting standard deviation was shown.

3.3.2 Light Transmission

The effect of the wavelength on the transmittance of five laser sintered polyamide 12 plates is shown in Figure 30. Four plates were processed by cyanoacrylate infiltration or polish, or both. Plate thicknesses were very similar, ranging from 1.79 to 2.06 mm. Measurements were made on four wavelengths presenting four monochromatic colors: 460 nm (red), 540 nm (green), 580 nm (yellow) and 640 nm (blue). The range of transmittance was 7% to 30%. Transmittance first increased linearly from 460 nm to the peak on 540 nm, then dropped to the lowest at 580 nm, and then increased a little at 600 nm.

At a constant wavelength, the cyanoacrylate infiltration on one surface plate showed the largest transmittance, followed by cyanoacrylate infiltration on two surfaces plate, non post processed plate, both faces polished plate, and one surface polished plate. The transmittance variations at the same wavelength were less than 5%.

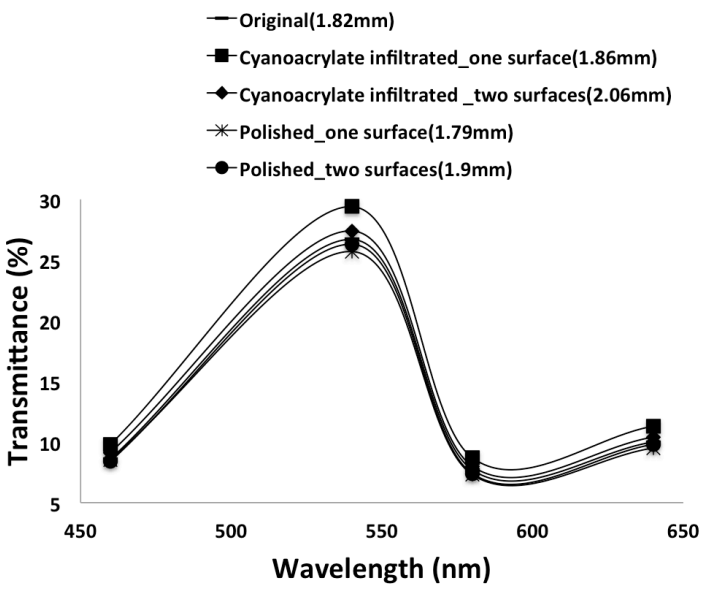

Figure 30: Effect of spectrophotometer wavelength on transmittance of laser sintered polyamide 12 surface finished by infiltration with cyanoacrylate and polished.

3.3.3 Plates performance comparison

Photos were taken of the non-post processed plate, one face polished plate (unpolished face on top, then polished face on top) and both faces polished plate using the white light box. The non-post processed plate in Figure 31 had a rougher surface finish comparing to the both face polished plate. More small pimples were presented on the non- post processed plate. The one face polished plate had a rough surface finish with the unpolished face on top, and had a better, smoother and finer surface quality with the polished face on top.

(a)

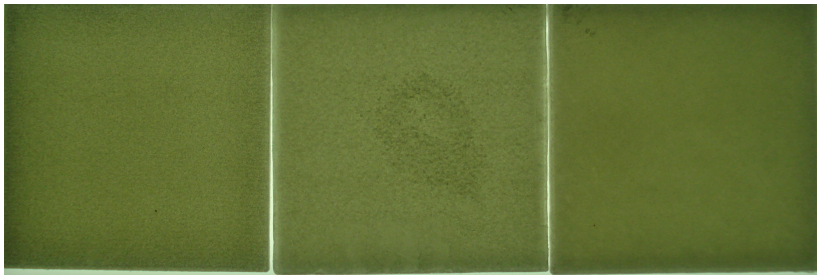

(b)

Figure 31: Photos taken on the light box for laser sintered polyamide 12 plates from left to the right: (a) non-polished and non- cyanoacrylate infiltrated standard, one face polished (unpolished face on top), both face polished; (b) non-polished

and non- cyanoacrylate infiltrated standard, one face polished (polished face on top), both face polished.

3.4 LITHOPHANE ORIENTATION VS. LIGHT SOURCE

Figure 32c shows a digital image of Dr. David Bourell; 32a shows the resulting backlit laser sintered polyamide 12 lithophane and 32b shows the digitally flipped lithophane photo facing the incident light. The quality of the image was substantially improved by orienting the flat plate side to the incident backlit light shown in Figure 32a. The image appeared blurred when the topographical side was oriented to the incident light as Figure 32b.

(a) (b) (c)

Figure 32: (a) laser sintered polyamide lithophane backlit with the grayscale topography facing the viewer (b) and facing the incident light (digitally flipped) (c) the digital image. Dimensions are 127 by 76 mm.

3.5 LITHOPHANE MANUFACTURING ORIENTATION

Figured lithophanes were fabricated with layer thickness 0.1016 mm, maximum plate thickness 3.81 mm, built on the ZX, YZ, and XY planes in the SinterStaton HiQ chamber, captured using the light box source shown in Figure 33. Better contrast and finer surface quality were shown on the ones built on the ZX an YZ planes compared to the one built on the XY plane. The backgrounds and figure jackets on the first two were more identifiable and fewer contours were shown. Also, the features on the face and hands were clearer. The hair shape, collar, and tie shape on the third lithophane was blurry, but they were legible on the lithophanes built in the ZX and YZ orientations.

Figure 33: Figured polyamide 12 lithophanes laser sintered with 0.1016 mm of layer thickness built in the ZX, YZ, and XY planes from left to the right. Maximum plate thickness was 3.8 mm. Lithophane photos were captured using the white light box source.

Chapter 4: Discussion

Eight sections are included in this chapter. First laser sintered polyamide 12 optical properties are analyzed, including light transmission and absorption. Wavelength dependent experiments were conducted to verify the optical property results. Second laser sintered lithophane manufacturing issues are discussed, including an analysis of thickness correction when building in the XY plane, discussion of the effect of layer thickness and maximum plate thickness on lithophane manufacture, and error analysis for the whole processes from the digital photo to manufacturing. Third, surface finish effects are discussed, light transmission through post processed blanks and non post processed blanks are reported, and plate performance are discussed.

Fourth, the laser sintered lithophane orientation versus the light source direction is analyzed. Fifth, the lithophane manufacturing orientation effects are examined. Wedges and plates with small features are sintered in different planes for defining manufacturing resolution.

Sixth, the material and time consumption are considered relative to different manufacturing orientations. Seventh, discussion of lithophane quality improvements is provided. Good LS lithophane quality definition and material selection criteria are established. Consideration of how to make a successful lithophane with LS using polyamide is given. Different laser sinterable materials were evaluated based on the selection criteria. Last, blanks and lithophanes made using stereolithograhy (SL) technology were analyzed and compared with those made using LS.

4.1 OPTICAL PROPERTIES

4.1.1 Light Transmission

In Figure 16 and 18, more photons were absorbed in a thicker blank plate, resulting in less light transmitted and more light absorbed**.** Only two kinds of electronic transitions lead to absorption in polyamide in the visible spectrum: n-pi* transition and pi-pi* transitions (Mattice, *et al*., 1994; William et al., 2004). The n-pi* transition corresponds to the excitation of an electron from one of the unshared pair to the pi* orbital and occurs at lower energy (high wavelength, 500-600 nm). It resulted in high transmittance and low absorbance. The pi-pi* transition corresponded to transition of electrons from a pi-bonds orbital to an antiboding pi orbital, which occurs at higher energy (lower wavelength, 300-400 nm), resulting in low transmittance and high absorbance (Mattice, *et al*., 1994; William et al., 2004).

High absorbance leads to low transmittance as seen by Equation 9. It is proposed that the pi-pi* transition is responsible for the transmittance increment from 400-540 nm, while the n-pi* transition explains the transmittance decreasing from 540- 580nm.

Based on Equation 10, absorption coefficients were solved (shown in Figure 21) and substituted into Equation 11. Results presenting the calculated transmittance are shown in Figure 17. The calculated results fit well with experimental results.

4.1.2 Light Absorption

Figure 18 is an inverse trend compared to Figure 16. Figure 19 shows the laser sintered polyamide12 blank plate logarithm of transmittance as a function of plate thickness under different monochromatic light: green, red, yellow and blue. The relation between ln (T) and plate thickness was linearly modified by applying the theoretical calculated intercept (-0.091) using Equation 5. This is shown in Figure 20. The slope is the negative of the absorption coefficient, which changes with transmitted light wavelength.

Figure 21 presents the absorption coefficients versus wavelength for laser sintered polyamide 12 plates. The absorption coefficient decreases in the wavelength range of 400 to 540 nm due to the pi-pi* transition, increased at 560-580 nm wavelength due to the n-pi* transition, then remains almost constant. This trend is consistent with Figure 16, indicating that a large absorption coefficient leads to low transmittance.

4.1.3 Wavelength Dependence Experiment

The transmittance trends in Figure 17 are verified on Figure 22 which showed large visual differences on the actual lithophanes. The photo was a reproduction of Raphael's sketch, 'Agnolo Doni'. The lithophane shows larger contrast and more light transmittance under green transmitted light than under yellow light, which was consistent with the transmittance shown in Figure 16.

Comparing the lithophane to the digital image, more contours were observed on the background, and the figure face was blurry due to the shortage of grayscale levels. There were only 37 layers of grayscale when sintering in the XY plane with alayer thickness of 0.1016 mm and maximum plate thickness of 3.81 mm, compared to 256 layers of grayscale on the initial image.

4.2 LASER SINTERED LITHOPHANE MANUFACTURING

4.2.1 Quantized Thickness Correction in the XY Plane

Figure 23 shows the corrected thickness for laser sintered polyamide 12 versus the software converted thickness under the monochromatic green light and white light. The relation that the conversion software used is shown by the dotted line. Both correction lines show larger thickness values compared to the uncorrected line after original height beyond 1.3 mm, which means for improved laser sintered polyamide 12 lithophane performance, the thick sections (>1.3 mm) need to be thicker. Moreover, the thickness increment rate was different depending on the light source.

Figure 24 illustrates the results from Figure 23 for two laser sintered stair-stepped lithophanes built in the XY plane. The corrected, upper sequence shows more uniform grayscale variation than the bottom sequence, especially from the second lightest square to the second darkest square, which validates the benefit for thickness correction within a 5 mm maximum plate thickness.

4.2.2 Layer Thickness

Comparing the lithophane performance using the white light box in Figure 25, the top sequence fabricated with 0.076 mm layer thickness showed improved contrast compared to the bottom sequence fabricated with 0.1016 mm layer thickness. With a constant maximum plate thickness, thinner layer thickness results in more grayscale levels on the lithophane.

For example, the thinnest feature on the laser sintered polyamide 12 lithophane was one layer thickness 0.1016 mm for parts fabricated with the layer thickness of 0.1016 mm. This was extrapolated to a transmittance of around 80% or a grayscale level of about 202 under the white light source (based on Figure 17). Here, one layer represents a drop of 255-202 = 53 grayscale levels. Theoretically, if the layer thickness could be reduced to 0.0254 mm, the transmittance would be around 90% or a grayscale level of about 230. Thus, the thinnest layer represents a drop of 255- 230= 25 grayscale levels. A comparison of the grayscale level lost on the thinnest layer with varying layer thickness is shown in Figure 34 below.

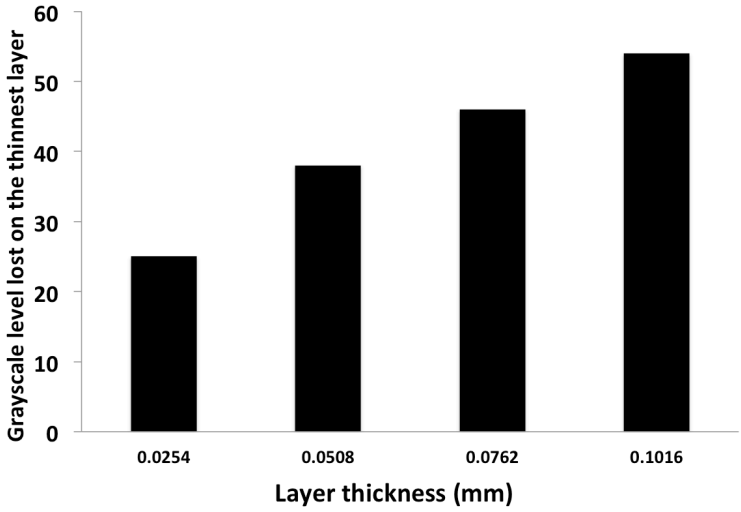

Figure 34: Grayscale level lost on the thinnest layer with different layer thicknesses: 0.0254, 0.0508, 0.0762 and 0.1016 mm.

Figure 34 shows that the layer thickness increases by four times from 0.0254 to 0.1016 mm, the grayscale level lost roughly increases two times from 25 to 53. A equation was converted to calculate the ΔG with respect to the layer thickness t:

$$\Delta G = 255 - 255\ \frac{(1-R)^2 e^{-\alpha t}}{1-R^2 e^{-2\alpha t}} \qquad (12)$$

where R is related with refractive index of the material, and α is the absorption coefficient. In terms of the laser sintered polyamide 12 using a white light source, α is equal to 1.41/mm, and R is 0.04454. So Equation 12 could be rewritten as:

$$\Delta G = 255 - \frac{232 e^{-1.41t}}{1-0.002 e^{-2.82t}} \qquad (13)$$

Equation 13 indicates for laser sintered polyamide 12, it was impossible to reach 100% transmittance, or zero grayscale lost due to the material property. The minimum grayscale level lost with the thinnest layer would be around 23.

Based on the Beer-Lambert Law (Equation 4) behavior, the incremental drop in grayscale level associated with a single layer depends on the absolute thickness of the plate and drops as the plate thickness increases. With a constant layer thickness (0.1016 mm), at around 25% transmittance, the part is about 1 mm thick. Hence, one layer changes the grayscale level by about 4 levels. For a 3 mm thick part, the transmittance is only about 5%, but even here a layer changes the grayscale level by 2 levels.

Figure 35 shows the grayscale level per layer for different layer thickness and plate thickness for laser sintered polyamide 12 lithphanes. On 1, 3, and 5 mm plates, the minimum grayscale levels were 72, 13, and 0 with respect to Figure 17.

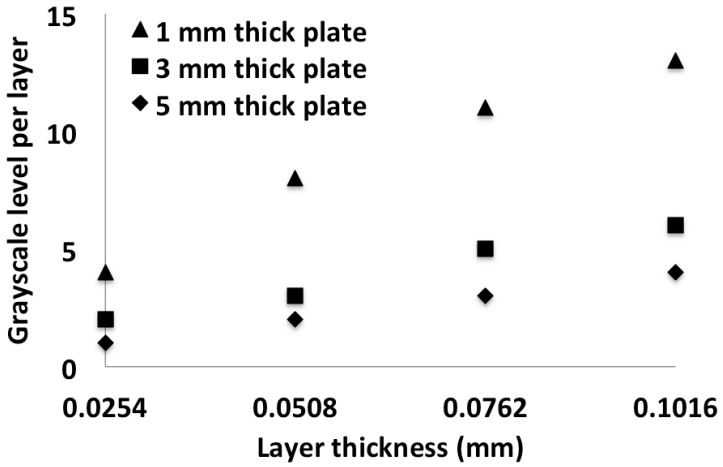

Figure 35: The grayscale level per layer for different layer thickness. (0.0254 to 0.1016 mm) and maximum plate thickness (1, 3 and 5 mm) for laser sintered polyamide 12.

Lithophanes with the same maximum plate thickness present a continuously larger grayscale level per layer with the increasing layer thickness, which is consistent with the lithophane performance in Figure 27. Lithophanes were presented with only 0.0762 and 0.1016 mm layer thickness due to the SinterStation fabrication limit. Thinner thickness layers result in a smaller grayscale levels per layer. Thus, more grayscale levels were present on the lithophane and resulted in better contrast, and more light transmitted through the lithophane.

An equation was created regarding to the grayscale level per layer G_{layer} regarding to the layer thickness t and plate thickness x. The total grayscale level presented was the difference between the grayscale level of plate thickness x and one layer thickness t:

$$G_{layer} = 255\left(\frac{t}{x}\right)\left(\frac{(1-R)^2 e^{-\alpha t}}{1-R^2 e^{-2\alpha t}} - \frac{(1-R)^2 e^{-\alpha x}}{1-R^2 e^{-2\alpha x}}\right) \quad (14)$$

In terms of laser sintered polyamide 12 with soft white light, the $R^2 e^{-2\alpha t}$ term is very small and may be taken to be zero. Substituting R and α into Equation 14:

$$G_{layer} = 232\left(\frac{t}{x}\right)\left(e^{-1.41t} - e^{-1.41x}\right) \quad (15)$$

Equation 15 indicates the grayscale level per layer was related with the layer thickness and maximum plate thickness. Small layer thickness and relatively large plate thickness results in a smaller G_{layer}, which produces better contrast in the lithophane.

4.2.3 Plate Thickness

Figure 25 shows large plate thickness leads to better contrast and improved quality of the lithophane. Figure 26 proves this assumption by presenting lithophanes on the white light box with 'extreme' absolute thicknesses of 1, 7, and 9 mm. These three lithophanes were built in the ZX plane.

Theoretically, the lightest feature produced in a laser sintered polyamide 12 lithophane is associated with a lithophane thickness of one layer. However, some structural integrity is necessary to allow handling and to prevent fracture by puncturing. For LS polyamide, this is 2-3 layers or a lithophane thickness of 0.15- 0.30 mm. Per Figure 17, for white light, the lightest feature then is associated with a plate thickness of 0.20 mm which yields a grayscale level of ~140 (~55% transmittance). This could in principle be improved by lowering the absorption coefficient α which may in turn be changed by selecting a different material or by using monochromatic light of appropriate wavelength.

Moreover, if the lithophanes become too thick, this causes problems with the topography becoming too distracting. Figure 36 illustrates this by presenting four lithophanes, with maximum plate thicknesses of 3, 5, 7, and 9 mm with a front lit white light source and black background. These four lithophanes are the same as the ones shown in Figure 25 and 26.

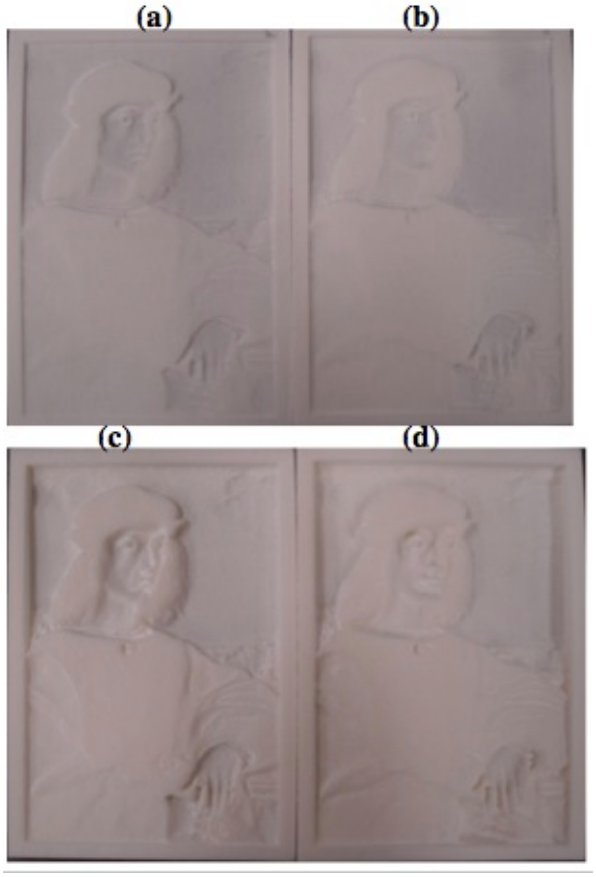

Figure 36: Lithophanes presented with the front lit white light source fabricated in the XY plane with the maximum plate thicknesses of (a) 3 mm and (b) 5 mm; fabricated in the ZX plane with the maximum plate thicknesses of (c) 7 mm and (d) 9 mm. All lithophanes were fabricated with a layer thickness of 0.1016 mm.

It is seen the bottom sequence shown clearer figure topography than the top sequence without the back-lit transmitted light source. The portrait could be obtained through the light reflection and scattering. Moreover, the transmittance was low since thick plate absorbed more light. Thus it lost the ideal of lithophane: translucent plate observed using a back lit light source.

Thus, there is also a limit on the maximum thickness of the lithophane, based on several considerations. First, there is a thickness associated with largely 0% transmittance. There is no improvement in grayscale darkness beyond this point by increasing the thickness. For LS polyamide (Figure 17) backlit by white light, this is 5 mm. Second, there is a cognitive limit to lithophane thickness, particularly if front lighting is present in addition to back lighting (which there usually is). If the lithophane were backlit in a black body, then there would be no front lighting. Otherwise, light will be incident on the front of the lithophane where presumably there would be a thickness profile to create the requisite contrast. If the plate is too thick, shadowing from the front lighting will detract from the transmitted light image. That is, a person will focus more on the topology variation made visible by the front lighting than the grayscale variations generated by the back lighting as in Figure 36.

In this case, for laser sintered polyamide 12 lithophanes fabrication with different maximum plate thicknesses varying from 1 mm to 9 mm, the optimal maximum plate thickness was obtained between 3.8 mm to 5 mm.

Lithophanes manufactured in the ZX plane had less contours on the background than those produced in the XY orientation as seen in Figure 26. Also the 1 mm thick lithophane fabricated on the XY plane in Figure 25 presented clearer portrait compared to the one fabricated on the ZY plane. The reason will be explained in the Section 4.5.

4.2.4 Error Analysis

A. Error caused by the layer thickness built in the XY plane

Figure 27 presents the small range correction at the region where original thickness was less than 1.3 mm, and Figure 28 shows the correction when the original thickness ranged from 1.3 to 4.9 mm.

The difference between theoretical height and nearest actual height based on available LS layer thickness would be reduced remarkably if the layer thickness were reduced from the regular 0.1016 mm to the minimum 0.0762 mm. However, the SinterStation could not reach the corrected height due to the manufacturing limit based on the available layer thickness as shown in Figure 37 below.

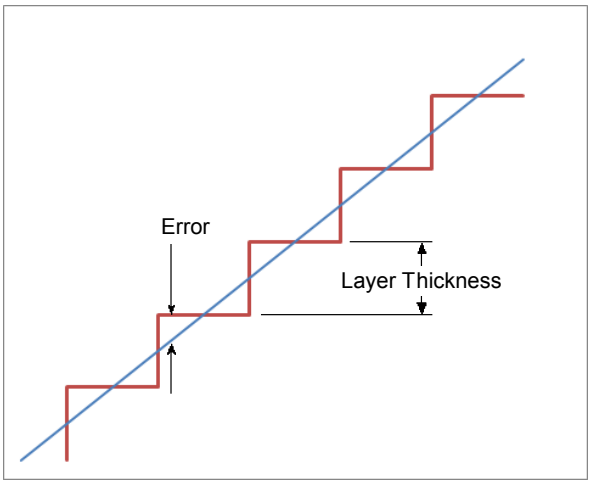

Figure 37: Illustration of the difference between the layer thickness and actual grayscale level.

The blue line in Figure 37 represents an actual grayscale level on an image, which was continuous; the red stair steps represent the layerwise AM process, which produces discontinuous grayscale levels. In LS, the layer thickness was on the order of 0.07 to 0.1 mm, which defines the actual number of grayscale levels that may be produced in a lithophane. This led to the error between the ideal grayscale level and the actual grayscale level.

Regarding to Figure 33, the grayscale level on the thinnest part (one layer) was 51. Therefore, it was not possible to accurately reproduce digital light grayscale features between 204 and 255, as they are associated with a thickness less than one layer.

Moreover, referencing Figure 34, the grayscale levels per layer for 0.1016 mm and 0.0762 mm layer thicknesses were between 3-13 at the maximum plate thickness near 5 mm. Thus, it was impossible to produce every grayscale level on the lithophane. However the 1 grayscale level per layer situation would be possible if the layer thickness reducing to 0.0254 mm while the maximum plate thickness was 5mm. Hence small stair steps (thinner layer thickness) result in less error between the ideal and actual grayscale levels, thus leading to more precision in creating an ideal thickness production.

However, the reality for LS polyamide lithophane production in the XY plane was that there were only about 50 levels of grayscale, associated with the 50 or so layers that span from one layer (0.1016 mm) at the thinnest to about 50 layers (5 mm) associated with zero transmittance.

B. Error caused by grayscale to thickness conversion

Simplistically, one might linearly interpolate a grayscale level (GSL) directly to a thickness using the maximum lithophane thickness as black (GSL 0) and one or perhaps two AM layers as white (GSL 255), reference Figure 6. More accurately, the grayscale level should be linearly related to the transmission T, and T is given by the Beer-Lambert Law as modified for transmission through a finite thickness plate (Equations 6 and 7). These approaches are illustrated schematically in Figure 38 for laser sintered polyamide 12. The solid line shows actual transmittance (or GSL) as a function of thickness. The simplistic approach to grayscale conversion produces large conversion errors depending on the maximum lithophane thickness.

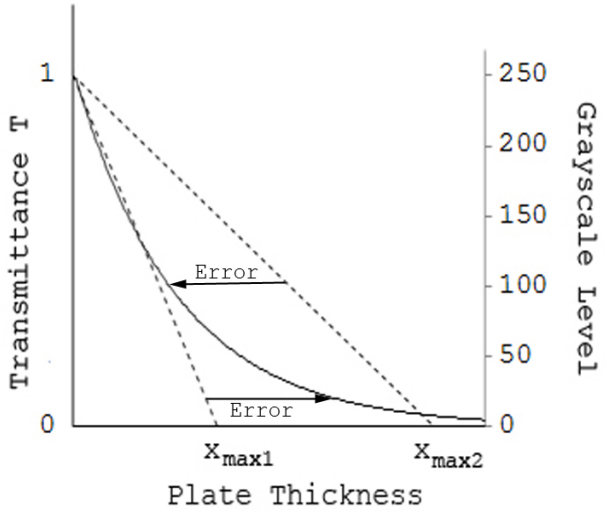

Figure 38: Schematic plot illustrating the Beer-Lambert Law of laser sintered polyamide 12 transmittance. x_{maxi} represents a maximum lithophane plate thickness.

If the overall lithophane thickness is near x_{max1}, then light features with high GSL are accurately reproduced, but there is a significant error in reproducing dark features near zero GSL. This error results in lithophane dark features being lighter compared to the digital image. If the maximum lithophane thickness is large compared to the extinction distance for the material as for x_{max2}, then dark features may be accurately reproduced, but there are large errors for mid-level features (e.g., GSL 50-200). In this case, the mid-level features would appear too dark (Yuan and Bourell, 2013).

Ideally, the conversion of grayscale to thickness would be based on the material's optical behavior such as Equation 10. This poses a complication though, because the software used to effect the conversion must include the optical behavior of the material to reduce the presenting errors, at least the absorption coefficient α and possibly the refractive index n. The latter defines the reflectance R according to Equation 3.

For most polymers, the refractive index ranges between 1.4-1.6, which results in Reflectance R less than about 5% (CES Edupack, 2012). The fact that AM part surfaces are generally rough improves light coupling which would further lower the reflectance. The result is that one might take $R \cong 0$, so that the Transmittance T becomes only a function of α. The ideal α value and ideal material are explored in Section 4.6.3.

C. Deviations from digital image

Deviation of the processed image from the original image occurred in all steps during the polyamide 12 lithophane production. The lithophane production flowchart and deviation situation is shown below in Figure 39.

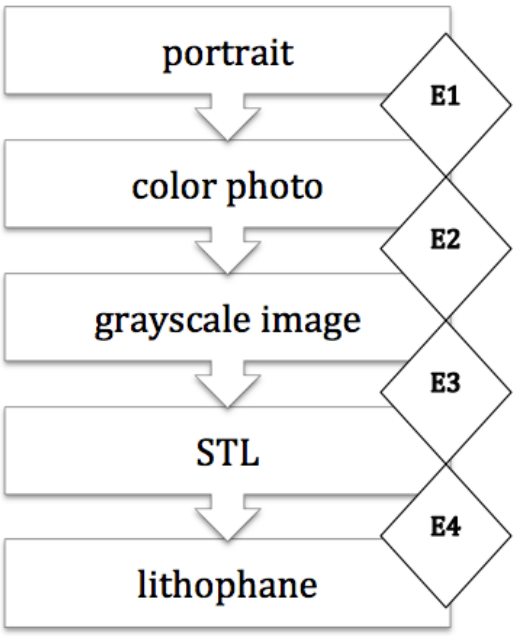

Figure 39: Flowchart showing the laser sintered lithophane production and deviation occurrence processes.

E1 is associated with taking the photo of the subject. Different kinds of camera lead to different levels of precision during photo capturing. Also, the way the photo is saced results in different error levels between the actual portrait and the digital image. JPG and BMP are the mostly common photo formats. JPG is a loss prone compression method for digital photography, which means the degrees of compression could be adjusted and typically achieved at 10:1. JPG supports 8, 16, and 24 bits color, which results in different saved sizes and quality. BMP files are generally uncompressed; hence, they are large. For example, the 'Agnolo Doni' used in this work reuqires 508 KB memory space when saved as a BMP and only 37 KB when saved as a JPG.

E2 comes from the conversion from a color image to the grayscale photo. The grayscale photo quality is reduced if the photo were processed in JPG format since the JPG suffers from generational degradation when repeatedly edited and saved. However, the BMP causes smaller error, but larger computer memory space is necessary. When converting the colored 'Agnolo Doni' into a grayscale image, the image size was reduced from 37 KB to 33 KB in JPG format, while it was maintained at 508 KB in the BMP format. Both E1 and E2 were a trade-off result from the memory size and the image quality.

E3 arises from the software that linearly converts the grayscale photo to the thickness and was discussed in Section 4.2.4 B. Also, the digital image pixel size would affect the lithophane thickness conversion because the pixel size defines the area dimension and thickness. Moreover, the software used here to convert the photo into the STL only handles image sizes smaller than 2 MB. It is noticed that the Bmp2Cnc is a experimental version software.

E4 is the manufacturing error during and after the LS. There was less than 1% error in product size when sintered on the SinterStation HiQ, and the error was enlarged to 5% when sintered in the SinterStation 2500. Also, the operating temperature and cool- down temperature result in varied product size errors because rapid cooling can cause distortion. Moreover, the part settlement was a manufacturing error taken into consideration. When manufacturing in the XY plane, the practical thickness was an integer of the layer thickness. Thus, there is a thickness difference between the ideal value and the obtained value. Last, the laser spot size limits the resolution of the lithophane. The DPI (dots per inch) was reduced from the original 150 to 25 pixels/inch during each lithophane production.

It is concluded that the total deviation for the manufacturing process was the sum of each error occurring during each step, from the photo taking to LS. It was proposed to use a higher resolution camera, save the photo in BMP file, decrease the laser spot size, and LS the part starting from an integer layer thickness to improve accuracy in lithophane production.

4.3 SURFACE FINISH

4.3.1 Surface Roughness Test

Figure 29 verifies the fact that polishing made the surface much smoother, thus improved the surface quality. And cyanoacrylate fills up some of the imperfections on the blank surface.

4.3.2 Light Transmission

Figure 30 shows that the transmittance of laser sintered polyamide 12 blanks sharing similar thickness was very similar, except the cyanoacrylate infiltrated on one surface plate presented 5% higher transmittance for 540 nm wavelength. It was reasonable that the cyanoacrylate infiltration prevented the photons from absorbing in the plate, leading to the highest transmittance on one surface cyanoacrylate infiltrated plate with a thickness of 1.86 mm, and the second highest transmittance on both surface cyanoacrylate infiltrated plate with a thickness of 2.06 mm.

Moreover, the transmittance range matched well with the transmittance showing in Figure 16. The post processes (infiltration, infiltration then polish) only dealt with the plate surface with no significant effect observed on the laser sintered polyamide 12 optical properties.

4.3.3 Plate Performance Comparison

In Figure 31, the left plate in both sequences is the non post processed laser sintered polyamide 12 plate, which has a rougher surface compared to the plate on the right, which was the cyanoacrylate infiltrated then polished on both surfaces plate. Tiny darker dots were observed on the left plate. The right plate showed smoother surface and more matte surface finish due to the polishing.

In terms of the one surface cyanoacrylate infiltrated then polished plate in the middle of the sequence, the two surfaces performed differently on the light box. It showed rough surface with dark dots on when the non-processed surface was on the top, and showed matte surface finish when the processed surface on the top. Since the lithophane grayscale topography surface had varying thickness, it was not possible to polish it, which means it is unlikely to have a smooth surface finish for the laser sintered polyamide 12 lithophane because the polish effect only worked on the polished surface.

4.4 LITHOPHANE ORIENTATION VS. LIGHT SOURCE

Lithophanes were created with one face of the lithophane plate flat and one with the grayscale topography. The quality of the image was substantially improved by orienting the flat plate side to the incident backlit light as shown Figure 32a. The image appeared blurred when the topographical side was oriented to the incident light as Figure 32b.

In this case, light was incident to the lithophane at varying surface angles which resulted in variable diffraction of the incident beam across the lithophane. This caused the image to blur. The diffraction was uniform when the flat side was presented to the incident light, which resulted in a sharper image.

4.5 LITHOPHANE MANUFACTURING ORIENTATION

4.5.1 Lithophane Performance Comparison on Thick Plate

Figure 33 shows that lithophanes with the same layer thickness and the same maximum plate thickness performed differently between fabricating on the XY plane and fabricating on the ZX or YZ planes.

Much clearer background and portrait were shown on the lithophanes built in the ZX and YZ planes. Lithophanes built in the ZX plane and XY plane were examined using stereomicroscopy with 2.5 X magnification on portrait tie and right middle cloud area as highlighted in Figure 15.

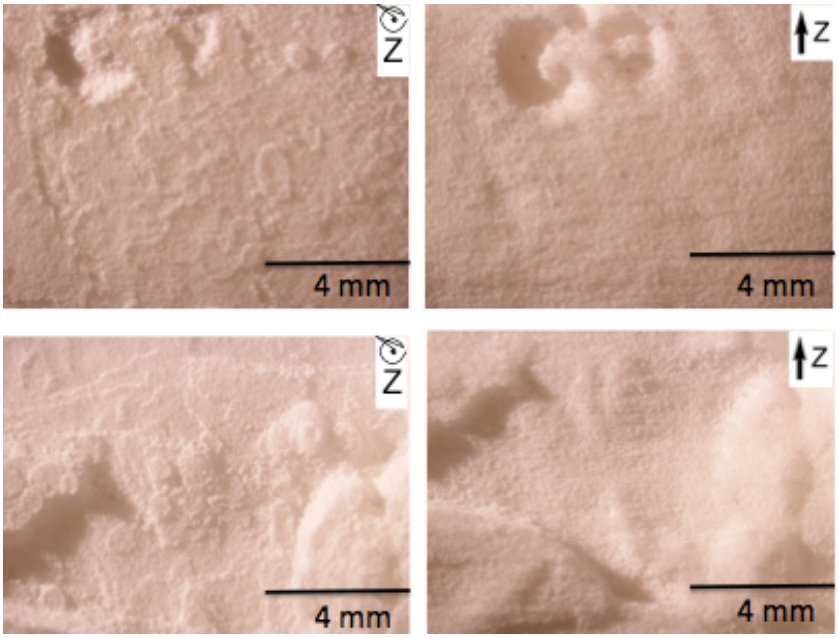

Figure 40: Stereomicroscopy photos of the lithophane focusing on portrait tie (top sequence); cloud on the middle right of the image (bottom sequence). The magnification was 1x. In both sequences, the left images were captured on the lithophane built in the XY plane, and the right images were captured on the lithophane built in the ZX plane.

The lithophane built in the ZX plane presents a much smoother surface and less contours than the one built in the XY plane. Layers were observed on the left images since the lithophane was built in the XY plane, with 38 layers in total (maximum plate thickness 3.8 mm and layer thickness 0.1016 mm). The layers appear like stairs (shown in Figure 37), and they define the grayscale levels. The grayscale level of the lithophane built in the ZX plane was defined by the laser beam motion, so it was continuous, and more levels were produced. Thus, the contrast comparison in Figure 33 was the comparison between 38 and effectively 255 grayscale levels.

4.5.2 Lithophane Performance Comparison on Thin Plates

Comparing the 1 mm lithophane performance shown in Figure 25 and 26, the ones built in the XY plane exhibited better contrast and resolution than the one built in the ZX plane. There were 13 and 10 layers on the lithophanes built in the XY plane with layer thicknesses of 0.762 and 0.1016 mm, respectively; however, the laser beam diameter was 0.5 mm, which was a half of the maximum plate thickness.

Thus it was impossible to create a fine portrait with a large diametric ‘pen’ on a thin ‘paper’. The situation would change with a thicker plate, since there would be more space for laser beam scanning. It is concluded then that it is preferred to LS the thin plate (1mm) on the XY plane instead of the Z plane.

4.5.3 Small Feature Characterization (ZX and YZ builds)

To analyze the laser beam effect on the smallest feature built with laser sintered polyamide 12, several bars with mini features (semi-cylinders and cuboids) and wedges were built in different directions and examined under stereomicroscopy using 10X magnification. Semi-cylinders and cuboids were built to track the laser beam scan path on different features while scanning in different directions. Wedge manufacturing was aimed at exploring the surface finish on very thin layers with different sintering orientations.

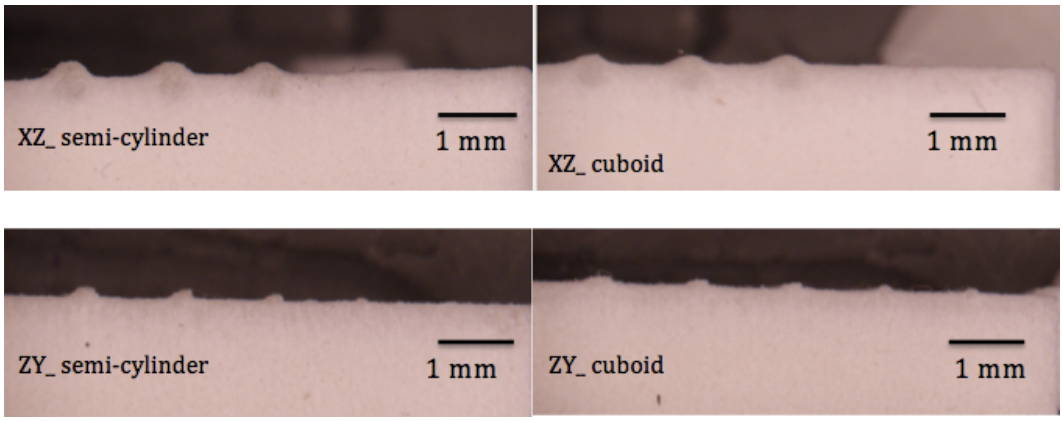

Figure 41: Stereo-micrographs for laser sintered polyamide 12 plates with small features under 10X magnification. The top sequence was the plates built in the XZ plane with semi-cylinder mounted on left, with cuboid mounted on right; the bottom sequence was the plates built in the ZY plane with semi-cylinder mounted on left, with cuboid mounted on right.

Only half of the plates are shown on each stereo-micrograph due to the lens limitation. Photos were taken from the end with the smallest features. Plates built in the XZ plane show three small features on both plates. The one mounted with semi-cylinders had diameters of 0.381, 0.508 and 0.635 mm and the one mounted with cuboids had the same value for the widths. Plates built in the ZY plane show five small features. The one mounted with semi-cylinders had diameters of 0.127, 0.254, 0.381, 0.508 and 0.635 mm and the one mounted with cuboids had the same value for the widths. The cuboids were not totally clear since the dimensions were too small (0.243 mm) for the laser spot to resolve, but the semi-cylinders show very well.

It is reasonable to achieve different feature resolutions depending on the manufacturing orientations. Figure 42 presents the top view of the build set up (Figure 11), which was the cross sectional area that the laser beam scanned over. The left two plates parallel with the Y-axis were built in the ZY plane, the plate with cuboid was on the left, and the plate with semi-cylinder was on the right side. Two plates on the right parallel with the X-axis were built in the XZ plane; the one mounted semi-cylinder was on the top while the bottom one was mounted with cuboid. The image was captured through Build Setup software created by 3D Systems.

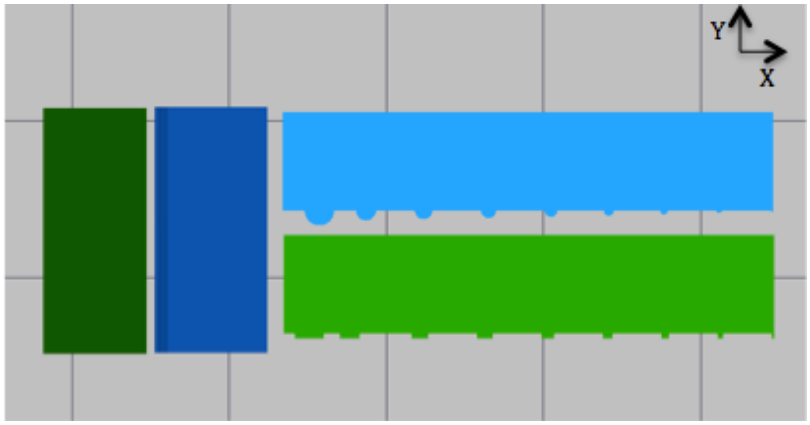

Figure 42: Top view of the build setup layout for plates with small features. The magnification was 3X with respect to Figure 11.

A slicer software was used to slice the STL files layer by layer so that laser could work on the cross section area. The left two plates had the cross section areas of rectangular with different widths, while the right two plates had the cross section areas of rectangular with small features on. The laser worked repeatedly on the direction parallel to X- axis first, then scanned parallel to the Y-axis on the next layer.

It is proposed through Figure 42 that the small features built in the ZY plane required laser beam line scan on rectangular while the ones built in the XZ plane required discontinued/ short line scan on irregular figures. Small features were more achievable with long scan lines, since it was continuous. Long line scanning on rectangular features also lead to more precision on positioning. Thus, small features with diameter or width of 0.127 mm could be produced.

It is concluded that the laser sintering resolution on the XZ plane for polyamide 12 was about 0.40 mm and the resolution on the ZY plane was 0.13 mm in terms of the building orientation in Figure 11.

To analyze the effect of layering and laser beam scan on very thin laser sintered polyamide 12 features, wedges were manufactured in four directions presented in Figure 12 and examined through stereomicroscopy under 10X magnification by the side view of the thin end (Figure 43) and the front view of the thin end (Figure 44).

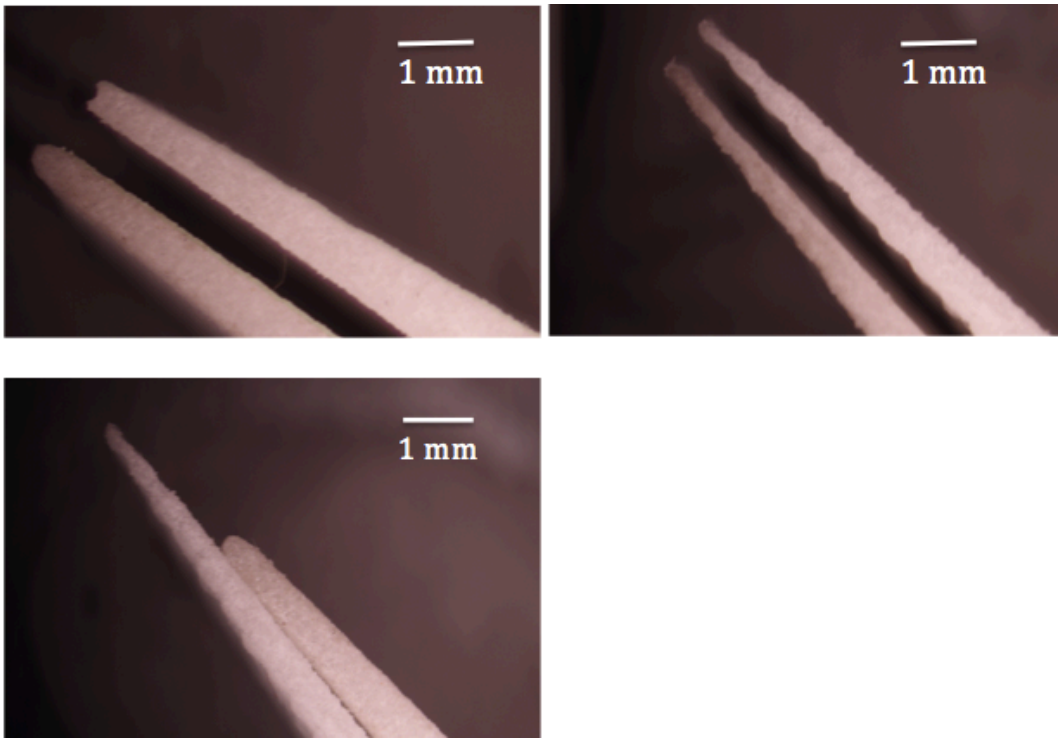

Figure 43: Stereomicrographs of laser sintered polyamide 12 wedges under 10X magnification. The stereomicroscope was focused on the side view of the thin edge. The first graph was the comparison between Sample 3 and 4 (referencing to Figure 12), the second was Sample 1 and 2, and the third was Sample 1 and 4. The photo was taken with the wedge bottom parts aligned.

Wedges built in the XY plane are shown in the first image of Figure 43. The top wedge was the one built with the flat surface up (Sample 3), while the bottom one was built with the flat surface down (Sample 4). The side view for each of the plate was similar, with a minimum thickness of 0.13 mm and total length of 100.20 mm for Sample 3 and 0.17 mm minimum thickness, 99.98 mm total length for Sample 4. The minimum thickness range was reasonable since the layer thickness was 0.1016 mm. Also measurement error (0.05 mm for the caliper) was included.

The second image of Figure 43 is the side view of the wedges built in the ZY plane, with layer thickness of 0.1016 mm. The top one was built with the flat surface down (Sample 1) and the bottom one was built with the flat surface facing up (Sample 2). Dimensions of these wedges were close, with the minimum thickness of 0.57 mm and total length of 94.90 mm for Sample 1 and 0.66 mm minimum thick and 95.02 mm long for Sample 2. The detailed results are shown in Table 6 below.

	Built in the ZX plane		Built in the XY plane	
Sample Number (Referencing to Figure 12)	1	2	3	4
Minimum tip thickness (mm)	0.57	0.66	0.13	0.17
Total length (mm)	94.90	95.02	100.20	99.98

Table 6: Comparison of minimum thickness on the thin end and total length for four laser sintered polyamide 12 wedge samples.

It is seen that the samples built in the same plane showed small difference on the dimensions. This was due to the layering issue during LS. The slicer software divided the part by each layer thickness, 0.1016 mm in this case, from top to the bottom. If the thickness value was between two layers, the software would choose the optimal layer number, thus leaded to variations on the actual part size.

The third image in Figure 43 presents the comparison between Sample 1 and 4. Obviously seen the wedge lengths were different. Sample 4 was 5.08 mm longer than Sample 1, and it showed more than three times thinner edge thickness, 0.17 mm compared to 0.57 mm. This was because the wedge thickness built in the XY plane relies on the layer thickness set from the SinterStation, which was 0.1016 mm in this study. However, the thickness was limited by the laser beam diameter (0.5 mm) when sintering the parts that stand vertically. Thus, the part thickness precision and length range were largely varied.

To compare the surface quality of the laser sintered polyamide 12 thin edges, stereomicrographs were captured on the flat surface under 10X magnification, per Figure 44.

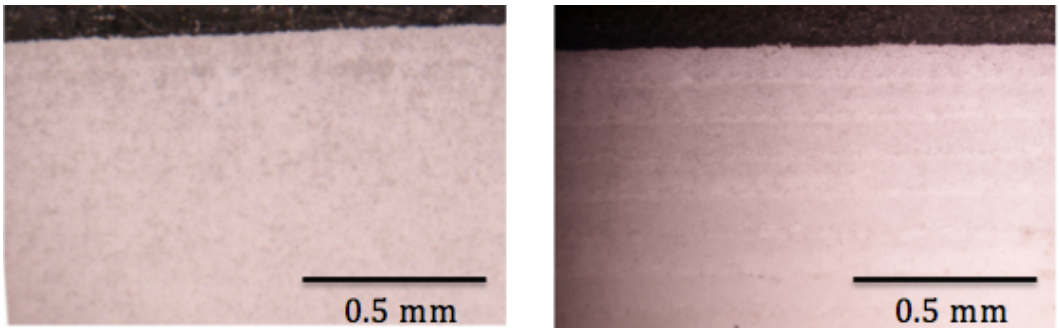

Figure 44: Stereomicrographs of laser sintered polyamide 12 wedges under 20X magnification. The stereomicroscope was focused on the thin hypotenuse flat edge. The left graph was the Sample 1(referencing to Figure 12), and the right graph was the Sample 3.

The photo on the left in Figure 44 is the stereomicrograph of Sample 1 and 2 hypotenuse surfaces front views on the thin tip. Both sample presented a smooth end, which implies that the manufacturing order and position did not have any effect on the part finish quality.

The second photo shows the front view of the thin hypotenuse surface for Sample 3 and 4, which were built in the XY plane. Horizontal lines present are the laser scan tracks. The distance between each track was 0.10 mm.

It is concluded that for LS on SinterStation HiQ, manufacturing on the Z plane results in better surface quality especially for the thin parts, but the thinnest feature size is 0.57 mm due to the laser beam diameter limitation. Manufacturing in the XY plane, the thinnest part would reach roughly one layer, but this is associated with poor surface quality on the very thin part.

4.6 CONSUMPTION ANALYSIS

To obtain the cost of material and time while manufacturing lithophanes using different orientations with different part quantity needed, several previews were run on the Build Setup software. The lithophane was 159 mm by 113 mm by 5 mm, which was a reproduction of the painting, 'Agnolo Doni'. The detailed comparison of manufacturing factors in different directions with respect to the lithophane and Sinstation HiQ are listed in Table 7.

The 'build set' refers to the build volume that associated with one lithophane Z direction orientation. The maximum number of parts per build set was calculated though dividing the building chamber dimensions in X and Y directions by the sum of the part dimension in X/Y- axis and the separation distance, taking the floor integers and multiplying them. The maximum number of build sets in a full chamber build was the floor integer obtained by dividing the total chamber height by the sum of the part height and separation layer distance.

		Building direction				
		XY	ZY	YZ	XZ	ZX
Preparation stage (warm-up, heat shield build, cool-down)	Time (hour)	2.67				
	Build height (mm)	17.20				
Separation layer	Time (hour)	0.11				
	Build height (mm)	2.54				
Part build (one)	Build height (mm)	5.16	158.85	113.51	112.62	158.85
	Time of Laser Scanning (hour)	0.14	0.45	0.25	0.39	0.26
	Time of feeding (hour)	0.29	7.68	5.52	5.42	7.81
Max number of lithophanes per build set		5	102	43	86	108
Max number of parts in a full chamber build		340	204	129	258	216
Unit time per part for full chamber build (hour)		0.24	0.55	0.40	0.45	0.36
Material used per part for full chamber build (kg) (part and surrounding part cake)		0.25	0.23	0.46	0.20	0.24
Material usage efficiency (%) (part mass/material used per part, full chamber build)		37.70	40.95	20.57	47.26	39.76

Table 7: Detailed comparison of manufacturing parameters between different building orientations.

There was 12.7 mm height of SinterStation warm-up stage and 2.54 mm height of cool-down stage in every build. Also a heat shield was built before the parts were sintered. The separation distance between each part was 2.54 mm to prevent over sintering with powder spread over the part bed surface without any lasing. The operation times for warming up, cooling down, separation layers, lithophane fabrication in each direction, and the powder feeding for one complete lithophane were simulated through the Build Setup software.

There was large quantity difference between building in the XY plane (5 per layer) and building in the ZY (102 per layer), ZX (108 per layer), XZ (86 per layer) or YZ (43 per layer) planes. Also, the available building layer number was different because of the part positioning. It is summarized that building in the XY plane led to the maximum plate quantity in a full build of 340 plates, and building in the XZ plane ranked second with 258 plates, building in the ZX plane ranked the third with 216 plates, followed by building in the ZY plane (204 plates) and YZ plane (129 plates). The situation will change if the different part dimensions vary.

The unit time per part for full chamber build was calculated by dividing the SinterStation operating time for the total lithophanes by the parts number. The SinterStation operating time on different manufacturing orientations with a maximum of 500 parts quantity is shown in Figure 45.

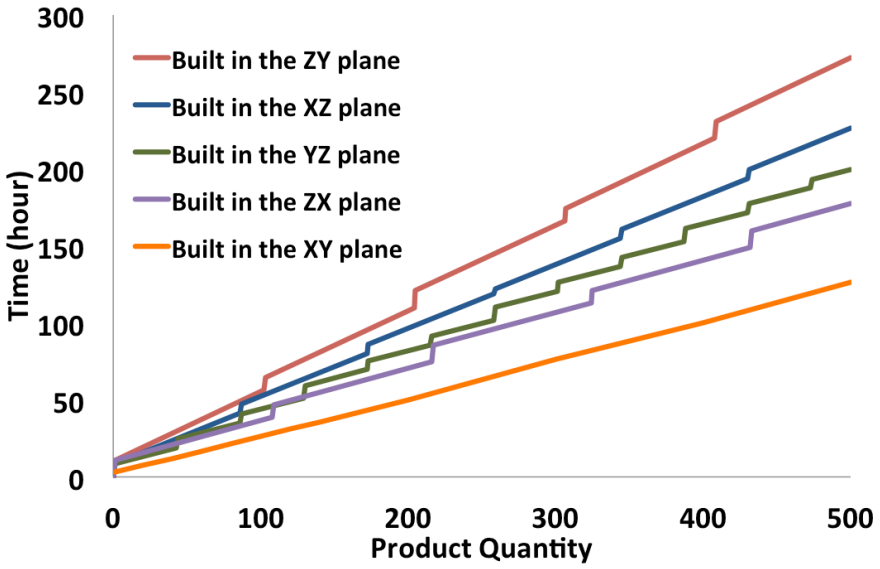

Figure 45: Product quantity versus time with respect to ZY, XZ, YZ, ZX, and XY building planes when laser sintering polyamide 12 lithophane on the SinterStation HiQ. The lithophane was a reproduction of 'Agnolo Don' with dimensions of 159 by 113 by 5 mm. The HiQ SinterStation has a build volume of 334.mm by 282 mm by 457 mm.

Figure 45 was obtained by calculating the time consumed in building different orientations based on Table 7. The time jump within one full build was smaller than that needed for starting a new build since new builds require time to warm up and build the heat shield and separation layers.

The total time consumption rate was roughly proportional to the building time per part, which was related to the cross-sectional area graphic feature of the lithophane. The laser scan time per lithophane on the ZY plane was the longest (0. 45 hour) compared to the other ones (0.39 hour for the XZ plane, 0.25 hour for the YZ plane, 0.26 hour for the ZX plane and 0.14 hour for the XY plane).

Powder feeding part bed time was the longest when manufacturing in the ZY plane (7.68 hour) since the powder quanitity needed for sintering one vertically standing lithophane was the largest, compared to 5.52 hour for the XZ plane, 5.42 hour for the YZ plane and 0.293 hour for the XY plane (reference Table 7). Building in the ZX plane was an exception. The powder feeding time was long (7.81 hour), but total time consumption was the second lowest due to the fact that the quantity of the maximum parts per layer was the largest among all five building orientations and the laser scan time per part was short (0.26 h), thus less total time was consumed. The unit time per part had the same trend with the total time consumption.

With respect to build time per part, lithophanes performed similarly with building in the ZY, ZX, YZ and XZ plane, and all had much better surface quality than building in the XY plane. So it was optimal to build in the ZX plane since less time consumption was needed.

The material used per part for a full chamber build was obtained by dividing the total powder usage by the produced part quantity. The total material usage was calculated and presented in Figure 46. The material usage efficiency was the ratio of the actual weight per lithophane to the material used per part for a full chamber build. In this case, the actual weight per lithophane was 0.095 kg.

Figure 46 shows the product quantity versus material consumption on the YZ, ZY, ZX, XY, and XZ planes, building the specific lithophane on the SinterStation HiQ. The calculation was based on the material cost for every step (warm-up, heat shield building, separation layering, cool-down) simulated in the Build Setup software shown in Table 7.

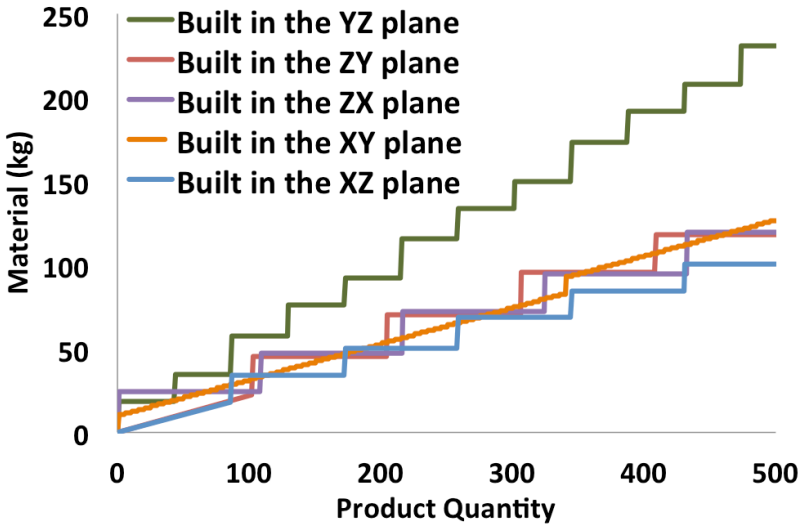

Figure 46: Product quantity versus material consumption regarding to ZY, XZ, YZ, ZX and XY building planes when laser sintering polyamide 12 lithophane on the SinterStation HiQ. The lithophane was a reproduction of 'Agnolo Don' with dimensions of 159 by 113 by 5 mm. The HiQ SinterStation had a building chamber of 333.451 by 282.067 by 457.2 mm.

Figure 46 shows the material consumption order from the highest to the lowest is building in the plane: YZ, ZY, ZX, XY, and XZ. This was relative to the maximum parts per full building, considering there were only 129 parts when building in the YZ plane, compared to 204 in the ZY plane, 216 in the ZX plane, 340 in the XY plane, and 258 in the XZ plane per full build. It was reasonable that the material consumption efficiency per part was the inverse trend; thus, building in the XZ plane achieved the highest material efficiency while building in the YZ plane reached the lowest because it reached the highest material consumption in Figure 46.

It is concluded that for the specific dimensional lithophane as used in this study, taking the time and material consumption into consideration, it was optimal to build either in the XZ plane or the ZX plane. The situation would change with different part dimensions and manufacturing requirements.

4.7 IMPROVEMENT OF LITHOPHANE QUALITY

4.7.1 Fine LS Lithophane Quality Definition

Based on the lithophane analysis in this work, it is proposed that a 'good' lithophane indicates the lithophane appearance (brightness, contrast and resolution) under the backlit light source is close to the look of the original digital image.

The light transmittance should be high (> 70%) at the thin areas and low (< 15%) at the thick sections. Largely varied brightness and darkness could then be shown on the lithophane, which enhances contrast. Second, the differences between each grayscale level/ thickness would be small, which leads to more continuously varied thicknesses. This in turn results in a vivid three-dimensional view on the lithophane. Third, the lithophane maximum plate thickness should fall within a range, below which would be too few grayscale levels, and beyond which the lithophane topography would be too obvious. Fourth, the resolution (or pixel size) of the lithophane should be relatively high, indicating fewer contours caused by the layering on the topography.

4.7.2 Laser Sintered Polyamide 12

Several manufacturing preferences are necessary for optimal performance of laser sintered polyamide 12 lithophanes:

- If manufacturing the lithophane in the XY plane, thinner layer thickness results in better contrast and more grayscale levels.
- Building in the Z plane is optimal for obtaining higher resolution and more continuous grayscale levels when producing plates greater than 2 mm thick.
- Building in the XY plane is optimal when producing thin plates less than 1 mm.
- Laser sintered polyamide 12 lithophanes have the best contrast and the most light transmission under green monochromatic light, and it is poorest under yellow monochromatic light.
- The laser sintered PA 12 lithophane maximum plate thickness range is around 3.8 to 5.0 mm. Beyond 5.0 mm, the topography would be easily observed optically which detracts from the transmitted image.

- The resolution of the lithophane depends on the SinterStation laser beam diameter when built in the Z plane and it depends on the single layer thickness when built in the XY plane.

- When building the plate with small features, it is best to place the plate in an orientation that shows a simper cross sectional area topography to the laser beam which leads to higher manufacturing resolution.

- Building the lithophane in the XZ or ZX plane consumes less material and time when the quantity requirement is large (>50).

- Surface polishing of the lithophane flat surface did not have any significant effect on lithophane quality.

4.7.3 LS Material Selection for Lithophane Production

A. Selection criteria

Based on the Beer-Lambert Law, material transmittance varies with the material reflectance, absorption coefficient and the plate thickness. The absorption coefficient varies with the transmitted light wavelength. While the thermoplastic refractive index ranged between 1.4 to 1.6, the reflection was small (2- 5%) calculated using Equation 3. Thus, the absorption coefficient α and plate thickness t are essential in determining the transmittance, as shown in Figure 47.

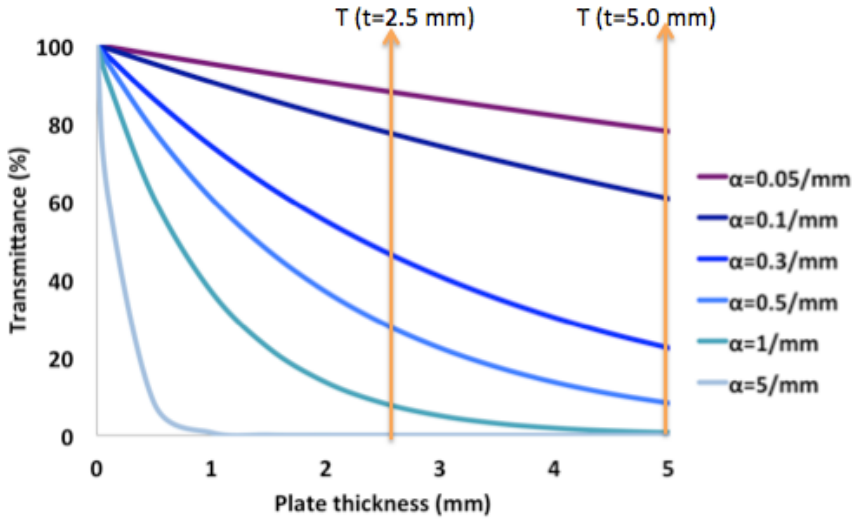

Figure 47: Theoretical plot of material transmittance versus plate thickness with different absorption coefficients ranging from 0.05 to 5/mm. The transmittances at 2.5 mm and 5 mm thick plates were highlighted. The reflectance was assumed to be zero. The plot was based on Equation 7.

In Figure 47, 5 mm thickness was selected as the largest thickness of the lithophane. It is seen that transmittance decreases with increasing plate thickness. The decreasing trend was exacerbated by increasing α. Moreover, the transmittance at 2.5 mm thickness was influenced by the transmittance at 5 mm thickness.

In ideal laser sintered lithophane manufacturing, it is desired to be very dark on the thick part and relatively bright on the thin part under the white light source, which means the transmittance at 5 mm thickness needs to be small, while at 2.5 mm thick the transmittance is relatively large. The relation between theoretical absorption coefficient and transmittance is shown in Figure 48.

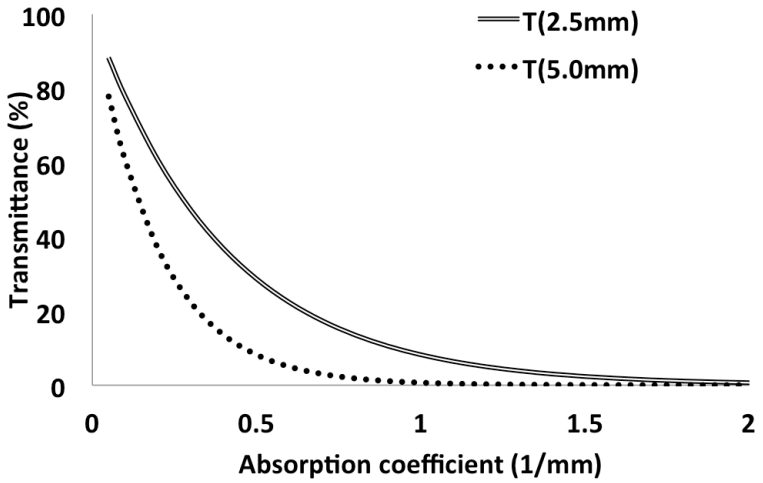

Figure 48: Theoretical plot of material transmittance versus absorption coefficient with plate thicknesses of 2.5 and 5 mm.

To obtain both relatively large T at 2.5 mm plate thickness and low T at 5.0 mm plate thickness, 0.5/mm was selected as the ideal material absorption coefficient for a white light source. The transmittance is roughly 30% at 2.5 mm thick, and 8% at 5.0 mm thick.

The absorption coefficient is related to the extinction coefficient k which depends on the transmitted light frequency:

$$\alpha = \frac{4\pi k}{\lambda} \qquad (16)$$

where λ is the transmitted light wavelength. k is related with the refractive index by

$$\tilde{n} = n + ik \qquad (17)$$

where the real part n indicates the phase speed, while the imaginary part k (extinction coefficient) indicates the amounts of absorption loss when the electromagnetic wave propagates through the material. In most circumstances, $k>0$ means light is absorbed and $k=0$ corresponds to light travelling without loss. $k<0$ means an amplification of the light.

Instead of finding an absorption coefficient, the goal turns to obtain the optimal extinction coefficient under specific light wavelength for candidate materials. The visible light wavelength range (400-800 nm) and absorption coefficient (0.5 /mm) are substituted into Equation 16, and the ideal extinction coefficient range for LS lithophane production is obtained: 1.59×10^{-5} to 3.18×10^{-5}.

B. Materials evaluation

A group of laser sinterable candidate materials were selected using the Granta Edupack materials selection software. The primary criteria included the polymer powder type (semi-crystalline or crystalline, thermoplastic) and melting point (160-200°C). The candidate polymers included EBA, EVOH, PA, PCL, PE, PP and PVDF. The detailed comparison is in Table 8.

	Extinction coefficient	Corresponding wavelength (nm)	Absorption coefficient (1/mm)	Reference
Criteria	1.59~3.18E-05	400-800	0.50	
EBA	5.04E-05	280	2.26	Peek *et al*., 2006
EEA	9.03E-05	488	2.32	Elke *et al*., 2008
EMA	2.00E-02	285	879.65	Takacs *et al*., 1995
EVOH	4.68E-03	360	163.36	Lasagabaster *et al*., 2006
PA	3.49E-05	540	0.69	Calculated results
PCL	1.56E-04	120	16.34	Choi *et al*., 2007
PE	2.40E-03	555	54.41	Klotz *et al*., 1984
PP	5.55E-04	370	18.85	Wiles *et al*., 1969
PVDF	6.00E-05	300	2.51	Solef®, 2012

Table 8: Comparison of extinction coefficients and absorption coefficients between candidate materials and selection criteria.

Table 8 shows polyamide 12 best fits the selection criteria for lithophane laser sintering, followed by EBA, EEA, and PVDF. It is proposed that nanocomposites might lead to improved properties by adding optical translucent nanoparticles into the base thermoplastic matrix.

4.8 OTHER AM PROCESSES

Stereolithography (SL) was performed in the Harvest Technologies® as an alternative lithophane production method to LS. The SL station, material, and relevant experiments are described.

4.8.1 Introduction to SL

A. Technology

SL is an additive manufacturing process that uses a photopolymer resin and a laser to build parts layer by layer. For each layer, the laser beam scans a cross section of the part pattern on the surface of the liquid resin. Exposure to the laser light cures and solidifies the cross section area pattern. The SL elevator platform then drops a distance equal to the single layer thickness, the resin-filled blade sweeps across the working area, re-coating it with liquid resin and the scan process is repeated until the total part has been built. After SL, the parts are immersed in a 99% ethanol to remove residual resin. They are then cured in an ultraviolet oven.

Supporting structures are used to attach the part to the elevator platform, preventing deflection due to the gravity and to hold the cross section in place. Supports must be removed from the cleaned product manually after the build is complete.

B. SL station

The SL station used in this research was the SLA® Viper ™ si2 from 3D Systems. A Nd: YVO_4 laser was used with wavelength of 354.7 nm and maximum laser power of 100mW. The vertical production resolution was 0.0025 mm, and typical scanning velocity is 50-100 mm/sec (3DSystems, 2003). The control software used was called Buildstation 5.3, which generates the STL file into the manufacturing station. Support structures were manually added in this software.

C. Material

DSM Somos®ProtoGen™ O- XT 18420 is a white, liquid, ABS like, epoxy resin photopolymer. It has good chemical resistance, wide processing latitude and tolerance to a broad range of temperature and humilities. It has a viscosity of 350cps at 30°C and density of 1.13 g/cm^3 at 25°C (Quickparts).

4.8.2 Experimental Procedure

Two lithophanes and one stair plate were built with the layer thickness of 0.1016 mm and laser power 57 mW at room temperature. The three-stair plate was built in the XY plane, with the thin part of 2.54 by 2.54 by 0.34 mm, the middle part of 2.54 by 2.54 by 1.06 mm, and the thick part of 2.54 by 2.54 by 5.11 mm. Two lithophane sizes were 127 by 76 by 5 mm. The photo was a reproduction of Raphael's sketch, Agnolo Doni. One lithophane was manufactured in the XY plane, while another one was manufactured in the ZY plane. All parts were immersed into 99% ethanol for 3 hours after being built; support structures were then removed manually by pinch.

Light transmission experiments were conducted on the three-stair plate under the monochromatic light wavelength in the range of 400 to 800 nm. The wavelength dependence experiments were performed under monochromatic blue and green lights, with the experimental settings the same as that for laser sintered PA 12 plate in Section 2.1.3. Photos were taken on both lithophanes with the soft white light box. Light transmission results and lithophane photos were compared with the laser sintered part results.

4.8.3 Results

A. Light transmission

The effect of the light wavelength on SL Somos® 18420 white resin transmittance is shown in Figure 49. Plate thickness ranged from 0.34 to 5.11 mm. Wavelength changed from 400 to 800 nm with 20 nm separations. The range of transmittance was 5% to 65%. Transmittance first dropped from the peak of 400 nm (65-50%) to 600 nm (14-4%). It then slowly increased from 600 nm to 800 nm (26-8%). At a constant wavelength, transmittance decreased monotonically with increasing plate thickness.

A very different transmittance trend is seen in Figure 49 for laser sintered polyamide 12 0.38 mm and 4.71 mm thick plates. Comparing the plates made with LS and SL, the LS plate (0.38 mm thick) had much higher light transmission than the SL plate (0.34 mm thick) from 460 to 800 nm light wavelength. The 4.71 mm LS blank had constantly lower transmittance than the 5.11 mm SL blank during all visible light wavelengths.

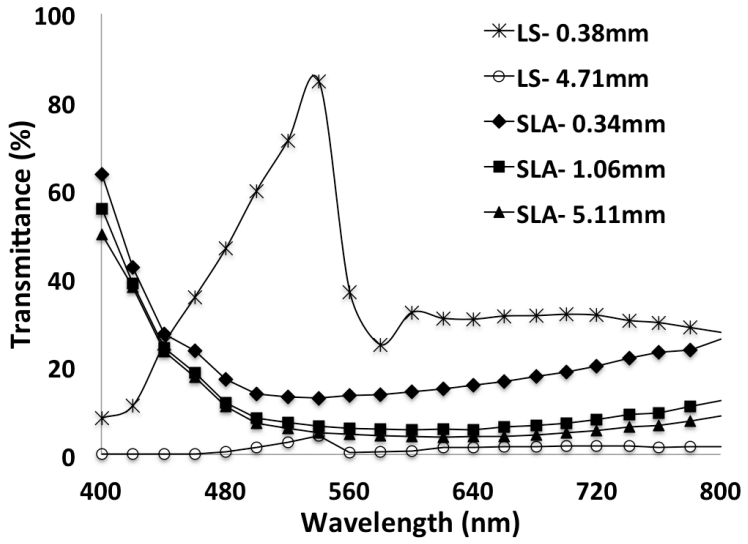

Figure 49: Effect of spectrophotometer wavelength on transmittance of SL resin plates with three different thicknesses. Also the transmittance of laser sintered 0.38 mm thick polyamide 12 plate is shown for comparison.

B. Light absorption coefficient

Absorption coefficients of SL Somos® 18420 were obtained in the same way as obtaining the absorption coefficient for laser sintered PA 12. The reflectivity of 5% and refractive index is 1.5 (SLA materials, 2013). Figure 50 shows the relation between the absorption coefficients versus wavelength for SL Somos® 18420 plates and LS polyamide 12 plates.

The Somos® 18420 plate absorption coefficient increases from 0.5 to 3 /mm in the wavelength range of 400 to 540 nm, then slowly decreases to 2/mm at 800 nm. This trend was consistent with Figure 49. Moreover, the Somos® 18420 plates showed consistently larger absorption coefficients than those for laser sintered PA 12 in the 460- 800 nm wavelength range.

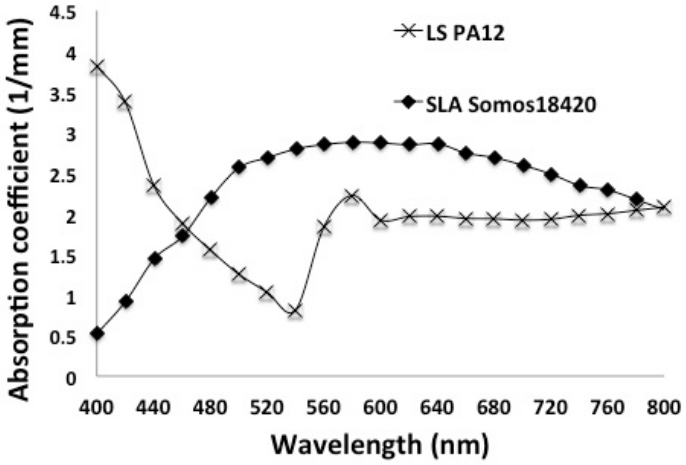

Figure 50: Plot of absorption coefficient versus transmitted visible light wavelength for SL resin and laser sintered polyamide 12.

C. Wavelength dependence experiment

Wavelength dependence experiments were conducted under the monochromatic blue light (wavelength 465 nm) and green light (wavelength 525 nm), seen in Figure 51. It is seen that the lithophane shows a larger contrast and better light transmittance under blue transmitted light than under green light, which was consistent with the transmittance shown in Figure 49. No contours were shown on the background, and a clear figure face and jacket tie were observed.

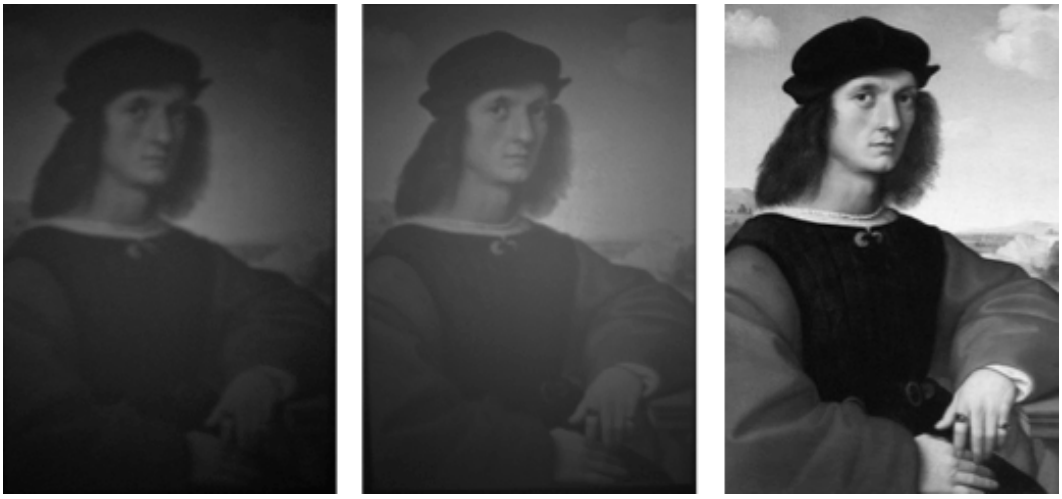

Figure 51: Gray-scale processed SL white resin 5.0 mm maximum thickness lithophanes under different monochromatic light with the same light intensity: green (left), blue (center). On the right was the initial digital image used to create the lithophanes.

D. Lithophane performance

Images on the left and middle in the Figure 52 show the figured lithophanes built in the XY and YZ planes use SL, with the maximum plate thickness of 5 mm with layer thickness of 0. 1016 mm. The image on the right is the lithophane built in the YZ plane using LS. SL lithophane boundaries and features on the figure face, tie, and hands were lucid. No contours were visible on the photos. Residual support structure was observed on the figure hands, especially in the middle image. The lithophane boundaries, figure jacket and hair were darker on the laser sintered lithophane.

Figure 52 : Figured SL lithophanes built in the XY plane (left); built in the ZY plane(middle); and figured LS lithophane built in the ZY plane (right). The maximum plate thickness was 5 mm. Lithophane photos were captured using a white light box.

4.8.4 Discussion

A. Light transmission

The SL Somos® 18420 plate shows a quite different transmittance trend compared to laser sintered PA 12. It is proposed that the energy needed for the electronic transition was low in the short wavelength range; thus, absorption was low and transmittance was high. The electronic transition energy was high at the long wavelength range, leading to high absorption and low transmittance.

The LS plate showed a high transmittance trend (maximum of 85%) on 0. 38 mm thick plate and constantly low transmittance trend (0-5%) on 4.71 mm thick plate, while highest transmittance for the SL plate was 65%, and the low transmittance trend was 5-50% on the 5.11 mm thick plate. There was greater transmittance variation on the LS plate, which resulted in improvement in contrast for the lithophane.

B. Light absorption coefficient

Figure 50 shows consistent resultss with Figure 49, indicating large absorption coefficient leads to low transmittance. Moreover, the constantly larger absorption coefficient of Somos® 18420 plate compared to PA 12 plate in the 460-800 nm wavelength range explains the lower contrast performance of SL plates compared to the PA 12 plates shown in Figure 52.

C. Lithophane performance

Lithophanes built with SL show clear detail and no contours on the background, due to the smaller laser beam diameter (0.2 mm) compared to that for LS (0.5 mm). Smaller laser beam diameter leads to more precise scan positioning and thus better lithophane appearance.

A significant amount of supporting structure was needed to prevent the 'vertical' lithophane from deflecting during the manufacturing process. This was difficult to remove completely due to the size of the tiny link construction and the complicated base topography on the figure hand.

Moreover, the contrast of the lithophanes manufactured with SL and LS varied, by observing the part boundaries and the figure jacket and tie. There was a

large variation in the partition of light transmitted through the lithophane, which was verified through Figure 50.

It is concluded that the lithophane made with SL using DSM Somos®ProtoGen™ O- XT 18420 white epoxy resin showed good and similar resolution when built in the XY or YZ plane with violet light (wavelength 400 nm) transmitting the most among all visible lights. However, the lithophane photo contrast was lower than that of the LS lithophane due to the low light transmission in the resin.

Chapter 5: Summary and Conclusions

The objective of this research work is to explore the laser sintered polyamide 12 optical properties, and optimal manufacturing methods for improving the laser sintered lithophane performances.

A series of experiments and analyses were conducted in this research work, including laser sintered polyamide 12 optical property analysis, laser sintered lithophane manufacturing study, surface finish experiments, lithophane orientation versus light source relation, lithophane manufacturing orientation research, consumption analysis, lithophane quality criteria consideration, improvement of lithophane quality, exploration of candidate laser sinterable materials for lithophane manufacturing, and other additive manufacturing technologies for producing lithophanes. Conclusions were drawn for each section:

Optical properties: Laser sintered polyamide 12 transmittance decreases with increasing plate thickness; transmittance reaches the highest levels under monochromatic green light. It reaches the lowest levels under yellow light.

Laser sintered lithophane manufacturing: When sintering in the XY plane, first the surface finish quality is improved by manufacturing with thinner layer thickness. Second, the maximum plate thickness affects the number lithophane grayscales, thus affecting the overall contrast. However, the total maximum plate thickness should not extend beyond 5 mm for laser sintered polyamide 12 the topography becomes be easily observed and detracts from the transmitted image. Third, in a small maximum plate thickness range, the difference between corrected thickness and the original thickness is smaller than one laser sintered layer, which results in thickness correction implementation difficulty. Fourth, in a large plate thickness range (<5mm), this error in correction between the ideal and original thickness is greatly reduced by reducing the layer thickness during the LS build, which benefits the surface finish quality. Last, thickness correction quantification on thick plates is effective to make the thick part look 'darker'.

Error analysis: It is concluded that errors occur during each process, from photo taking to manufacturing. Using a high-resolution camera, saving the photo as a BMP file, and laser sintering the part starting from an integer layer all help to eliminate the total error.

Surface finish: Cyanoacrylate infiltration and polishing greatly help reducing the laser sintered polyamide 12 plate surface roughness, but these processes do not change the material optical properties. Moreover, polishing does not affect the lithophane quality since the polishing effect may only be applied to the polished flat surface.

Lithophane manufacturing orientation: Sintering a thick lithophane in the Z plane significantly increases the contrast and resolution compared to sintering in the XY plane, because the laser beam scans along a continuous path to define the image topography. The thinnest feature thickness possible in the SinterStation HiQ is in the XY plane 0.13 mm with 0.1016 mm layer thickness, and it is 0.57 mm when manufacturing in the Z plane with the laser diameter of 0.50 mm.

Improvement of lithophane quality: It is preferred to build in the Z plane with maximum plate thickness 5 mm. When build in the XY plane, it is optimal to sinter with the minimum layer thickness (0.076 mm) and maximum plate thickness 5 mm. Laser sinterable material selection criteria were carried out, which required the material to have an absorption coefficient of 0.5/mm under a white light source, PA 12 was the best semi-crystalline material after comparison with a list of other semicrystalline and crystalline candidate materials.

Other AM Processes: Stereolithography was analyzed using Somos® 18420 white resin. Transmittance reached the highest levels under violet light, and it reached the lowest levels under the green light. Better resolution and poor contrast were observed compared to laser sintered lithophane.

Laser sintered lithophanes serve as an interesting and complex LS industrial application. Optical properties, manufacturing aspects, and other related issues were analyzed and discussed in this dissertation. Future work may include the use of nanocomposites for optimal lithophane performance, and more precise manufacturing processing to improve the lithophane resolution.

References

ALM PA 650 Techanical Data Sheet (09-28-2011), available on: http://alm-llc.com/Tech_Data_Sheets/PA_650.pdf, last access: 09-02-2013.

Ahn, S., Lee, C. S., Felong, W. (2004), "Development of translucent FDM parts by post-processing", *Rapid Prototyping Journal*, Vol. 10 No. 4, pp. 218-224.

Akova T., Ucar Y., Tukay A., Balkaya MC., Brantley WA., (2008), 'Comparison of thebond strength of laser sintered and cast base metal dental alloys to porcelain', *Dental Materials*, Vol. 24, Iss 10, pp. 1400-1404.

Bak, H., Cho, S. Y., Yun, Y. S., Jin, H. (2010), 'Electrically conductive transparent films based on nylon 6 membranes and single-walled carbon nanotubes', *Current Applied Physics*, Vol. 10, pp. 468-472.

Bertol LS., Junior WK., Silva FP., Kopp CA., (2010), 'Medical design: direct metal laser sintering of Ti- 6Al- 4V', *Materials & Design*, Vol. 31, Iss. 8, pp. 3982-3988.

Bourell, D.L., Marcus, H.L., Barlow, J.W., Beaman, J.J. "Selective laser sintering of metals and ceramics", *International Journal of Powder Metallurgy*, Vol. 28, No. 4, 1992, pp. 369-81.

Brown, W. H., Foote, C. S., Iverson B. L., (2004), *Organic Chemistry* , Brooks/ Cole, ISBN -13: 978-0534467739, pp.1037.

Bruno, T., J., Svoronos P. D. N., (2005), CRC Handbook of Fundamental Spectroscopic Correlation Charts, CRC Press, pp. 30-32.

Carlsson DJ., Wiles DM., (1969), 'The pohotodegradation of polypropylene films. III Photolysis of polypropylene hydroperoxides', *Macromolecules*, 2(6), pp. 597-606.

Carney, Margaret, (2007), Lithophanes, Schiffer Publishing, ISBN 978-0-7643-3019-3.

Choi WH., Johnson JK., Nam J., Farson DF>, Lannutti J., (2007), 'Structuring electrospun polycarprolactone nanofiber tissue scaffoldsby femtosecond laser ablation', *Journal of Laser Application*, Vol. 19, Numb. 4, pp. 225-231.

Crouch S., Skoog DA., (2007), 'Principles of instrumental analysis'. *Australia: Thomson Brooks/Cole*. Pp. 335- 398. ISBN 0-495-01201-7.

Deckard C, 'Method and apparatus for producing parts by selective sintering', *US Patent 4863538*, filed 10-17-1986, published 09-15-1989.

Dewidar MM., LIM JK., Dalgarno KW., (2008), 'A comparison between direct and indirect laser sintering of metals', *J. Mater. Sci. Technolo.*, Vol. 24, No. 2, pp 227- 232.

Diller T, Yuan M, Bourell D, 'Thermal Model and Measurements of Polymer in Laser Sintering', *Rapid Prototyping Journal*, accepted on 06-May-2013.

Douling, NE, 1993, Mechanical Behavior of Materials: Engineering Methods for Deformation, Fracture and Fatigue, Prentice-Hall, Englewood Cliffs, NJ.

Fouquaert E., Peumans W. J., Smith D. F., Proost P., Saccides S. N., Damme E. J. M. V., (2008), 'The 'old' euonymus eurpoaeus agglutinin represents a novel family of ubiquitous plate proteins', *Plant Physiology*, Vol. 147, No.3, pp. 1316-1324.

Gibson I, Shi DP, 1997, 'Material properties and fabrication parameters in selective laser sintering process', *Rapid Prototyping Journal*, Vol. 3 Iss: 4, pp.129 - 136

Gu D., Shen Y., (2009), 'Balling phenomena in direct laser sintering of stainless steel powder: metallurgical mechanisms and control methods', *Material & Design*, Vol. 30, Iss 8., pp. 2903-2910.

Greenham N. C., Samuel I.D.W., Hayes G.R., Phillips R. T., Kessener Y. A.R.R., Moratti S. C., Holmes A. B., Friend R. H. (1995), 'Measurement of absolute photolminesence quantum efficiencies in conjugated polymers', Chemical Physics Letters, Vol. 241, pp. 89-96.

Greskovich C., and Chernoch JP., 2009, 'Polycrystalline ceramic lasers', *Journal of Applied Physics*, Vol. 44, Iss 10., pp. 4599-4606.

Haase, P., "Selective laser sintering of metal powders", MS thesis, Center for Materials Science and Engineering, The University of Texas at Austin, Austin, TX, 1989.

Houze, Herbert G., (2006), Samuel Colt: Arms, Art, and Invention, Yale University Press, ISBN 0-300-11133-9.

Hughes J., Thomas R., Byun Y., Whiteside S., (2012), 'Improved flexibility of thermally stable poly-lactic acid (PLA)', Carbohydrate Polymers, Vol. 88, pp. 165-172.

Hunt R.W.G., (2004), 'The reproduction of color (6th ed.)', Chichester UK: Wiley-IS&T Series in imaging Science and Technology, ISBN 0-470-02425-9.

Jean-Baptiste-Ambroise-Marcellin Jobard, *Les nouvelles inventions aux expositions universelles* (Brussels and Leipzig, 1858), volume 2.

KH Tan, CK Chua, KF Leong, CM Cheah, P Cheang, MS Abubakar, SW Cha, 2003, 'Scaffold development using selective laser sintering of polyetheretherketonr-hydroxyapatite biocomposite blends', *Biomaterials*, pp. 15-23.

Klocke, F., Wirtz, H. (1997), 'Selective laser sintering of ceramics', *Proc. Int. Conf. Laser Assisted Net Shape Engineering*.

Klotz AV., Glazer AN., (1984), 'Characterization of the Bilin attachment sites in R-Phycoerythrin', *The Journal of Biological Chemistry*, Vol. 260, No. 8, pp. 4856- 4863.

K-MAC Plastics, 3821 Clay Ave. SW, Wyoming, MI 49548, Availabel at: http://k-mac-plastics.net/index.htm, last Access on: 21/08/2013.

Kruth JP, Wang X, Laoui T, Froyen L, 2003, 'Lasers and materials in selective laser sintering', *Assembly Automation*, Vol. 23 Iss: 4, pp.357 – 371.

Kruth JP., Froyen L., Vaerenbergh LV., Mercelis P., Rombouts M., Lauwers B., (2004), *J. Mater. Process. Technolo.*, 149, 616.

Lai S. M., Chen W. C., Zhu X. S., (2009), 'Melt mixed compatibilized polypropylene/clay nanocomposites: Part 1- the effect of compatibilizers on optical transmittance and mechanical properties', Composites: Part A, Vol. 40, pp. 754-765.

Lasagabaster A., Abad MJ., Barral L, Ares A.,(2006), 'FTIR study on the nature of water sorbed in polypropylene (PP)/ethylene alcohol vinyl (EVOH) films', *European Polymer Journal*, Vol. 42, Iss 1., pp. 3121-3132.

LaserSintering.com, 'SLS materias', available at: http://www.lasersintering.com/materials.php#; last access: 08-26-2013.

Leiggener C., Messo E., Thor A., Zeilhofer HF., Hirsch JM., (2009), 'A selective laser sintering guide for transferring a virtual plan to real time surgery in composite mandibular reconstruction with free fibula osseous flaps', *International Journal of Oral and Maxillofacial Surgery*, Vol. 38, Iss. 2, pp. 187-192.

Leong KF., Cheah CM., Chua CK, (2003), 'Solid freeform fabrication of three-dimensional scaffolds for engineering replacement tissues and organs', *Biomaterials*, Vol.24, Iss. 13, June 2003, Pages 2363 – 2378.

Liu F. R., Zhao. J. J., Zhang Q., He C. Chen J. M., (2012), 'Processing and characterizations of 2% PF/silica sand core-shell composite powders by selective laser sintering with a higher transmittance fiber laser', International Journal of Machine Tools& Manufacture Vol. 60, pp. 52-58.

Lu J., Prabhu M., Ueda K., Yagi H., Yanagitani T., Kudryashov A., Kaminskii AA., (2001), 'Potential of ceramic YAG lasers', *Laser Physics*, Vol. 11, No. 10, pp. 1053-1057.

Lu L., Fuh JY., Wong YS., (2001), 'Laser-induced materials and process for rapid prototyping', *Kluwer Academic Publishers*, Norwell, USA.

Macedo ZS., Hernandes AC., (2002), 'Laser sintering of $Bi_4Ti_3O_{12}$ ferroelectric ceramics', *Materials Letters*, Vol 55, Iss. 4, pp. 217-220.

Macedo ZS., Silva RS., Valerio MEG., (2004), 'Laser- sintered bismuth germinate ceramics as scintillator devices', *J. Am. Ceram. Soc.*, 87, [6], pp. 1076-181.

Manriquez-Frayre, A. and Bourell, D.L., "Selective laser sintering of binary metallic powder", in Beaman, J.J., Marcus, H.L., Bourell, D.L. and Barlow, J.W. (Eds), *Proceedings of the Solid Freeform Fabrication Symposium*, The University of Texas at Austin, Austin, TX, 1990-94, 1990, pp. 99-106.

Manriquez-Frayre, J.A. and Bourell, D.L.",Selective laser sintering of Cu-Pb/Sn solder powders", in Beaman, J.J., Marcus, H.L., Bourell, D.L. and Barlow, J.W. (Eds), *Proceedings of the Solid Freeform Fabrication Symposium*, The University of Texas at Austin, Austin, TX, 1990-94, 1991, pp. 236-44.

Mattice, W. L., Sutter U. W., (1994), Conformational Theory of Large Molecules, Wiley, New York.

Morrill TC., Silverstein RM., Bassler GC., (1981), 'Spectronmetric identification of organic compounds', *New York: Wiley*. ISBN 0-471-02990-4.

Mukesh A., Bourell D., Beaman J., Marcus H., Barlow J., (1995), /Direct selective laser sintering of metals', *Rapid Prototyping Journal*, Vol. 1, Num. 1, pp.26-36.

Niino, T., Yamada H. & Seki, S., 2004. "Preliminary Study for Transparentization of SLS Parts by Resin Infiltration", *Proc. SFF Symposium*, Austin TX, pp. 236-243.

Niino, T. & Yamada, H., 2005. "Transparentization of SLS Processed SMMA Copolymer Parts by Infiltrating a Thermosetting Epoxy Resin with Tuned Refractive Index ", *Proc. SFF Symposium*, Austin TX, pp. 208-216.

Peek L.J. Brabdau D.T., Jones L. S., Joshi S.B., Middaugh C. R., (2006), 'A systematic approach to stabilizing EBA- 175 RII- NG for use as a malaria vaccine', *Vaccine*, Vol. 24, Iss. 31-32, pp. 5839-5851. '

Quickparts. Com, 'Somos®ProtoGen™ O- XT 18420', available at: http://www.quickparts.com/UserFiles/File/SLA_Somos_18420.pdf, last access on 2013/10/09.

Raphel, (1506-1507), 'Portrait of Agnolo Doni'. Available at: http://en.wikipedia.org/wiki/Portrait_of_Agnolo_Doni; last access on 2013/11/18.

Rose R. M., Shepard L. A., Wulff J., (1965), 'The structure and properties of materials', Vol. iv, 'Electronic properties', John Wiley& Sons, pp. 271-290.

Rhim J., Hong S., Ha. C., (2009), 'Tensile, water vapor barrier and antimicrobial properties of PLA/nanoclay composite films', LWT- Food Science and Technology, Vol. 42, pp. 612-617.

'Selective Laser Sintering, Birth of an Industry', last updated: 05-30-2013, available at: https://www.me.utexas.edu/news/2012/0712_sls_history.php.

SLA materials, available at: http://www.forecast3d.com/sla_materials.html. Last access on: 2013/11/04.

'Standard terminology for additive manufacturing- coordinate systemsand test methodologies', ISO/ ASTM 52921: 2013 (E)

Stephen Johnson, (2006), 'Stephen Johnson on Digital Photography', O'Reilly, ISBN 0-596-52370-X.

Street G.B., Clake T.C, Krounbi M, Kanazawa K., Lee V, Pfluger P., Scott J.C., and Weiser G., (1981), 'Preparation and characterization of neutral and oxidized polupyrrole films', Molecular Crystals and Liquid Crystals, Vol. 83, Issue 1, pp. 253- 264.

Solef® PVDF, (2012), 'Design and Processing Guide', available at: http://www.solvayplastics.com/sites/solvayplastics/EN/Solvay%20Plastics%20Literature/DPG_Solef_Hylar_EN.pdf. Last access on 2013/10/09.

Song AK, Koening W., (1997), 'Experimental study of the Basic Process Mechanism for Direct Selective Laser Sintering of Low-Melting Metallic Powder', *CIRP Annals - Manufacturing Technology*, Volume 46, Issue 1, 1997, Pages 127 – 130

Sung S. I., and Sung W. B.,(1994), 'Preparation and properties of transparent and conducting nylon 6-based composite films', Journal of Applied Polymer Science, Vol. 51, pp. 1221-1229.

Sung W. B., Seung S. I., (1997), 'Physical properties and doping characteristics of polyaniline-nylon 6 composite films', Polymer Vol. 39, No. 2, pp. 485-489.

Suwanprateeb, F., Suwanpreuk, W. (2009), "Development of translucent and strong three dimensional printing models", *Rapid Prototyping Journal*, Vol. 15 No. 1, pp. 52-58.

Taboas JM, Maddox RD., Krebsbach PH, Hollister SJ, 2003, 'Indirect solid free form fabrication of local and global porous, biomimetic and composite 3D polymer- ceramic scaffolds', *Biomaterials*, Vol. 24, Iss. 2, pp. 181- 194.

Takacs E., Wojnarovits., (1995), 'Time resolved study of the high energy radiation initiated polymerization', *Nuclear Instruments and Methods in Physics Research B*., 105, pp. 282-284.

Tan KH., Chua CK., Leong KF., Cheah CM, Cheang P, Abu Bakar MS., Cha SW., (2003), 'Scaffold development using selective laser sintering of polyetheretheketone- hydroxyapatite biocomposite blends', *Biomaterials*, Vol 24, Iss 18, pp. 3115-3123.

Tang C., Liu H.(2008), 'cellulose nanofiber reinforced poly(vinyl alcoghol) composite film with high visible light transmittance', *Composites: Part A*, Vol. 39 pp. 1638-1643.

Tang H., Chiu M., Yen H., (2011), 'Slurry-based selective laser sintering of polymer-coated ceramic powders to fabricated high strength alumina parts', *Journal of the European Society*, Vol. 31, pp.1383-1388.

'Theory of ultraviolet-visible (UV-Vis) spectroscopy, available at: http://www.chem.ucla.edu/~bacher/UV-vis/uv_vis_tetracyclone.html.html. Last access on: 2013/11/15.

Traini T., Mangano C., Sammons RL., Mangano F., Macchi S., Piattelli A., (2008), 'Direct laser metal sintering as a new approach to fabrication of an isoelastic functionally graded material for manufacture of porous titanium dental implants', *Dental Materials*, Iss. 24, pp. 1525-1533.

Tobolsky, A.V. (1967), *Properties and Structure of Polymers*, John Wiley & Sons, New York, NY.

Tolochko N., Mozzharov S., Laoui T., Froyen L., (2003), 'Selective laser sintering of single- and two- component metal powders', *Rapid Prototyping Journal*, Vol. 9, Num 2, pp. 68-78.

Viper si2 SLA SYSTEM data file, available at: http://www.3dsystems.com/products/datafiles/viper/datasheets/International/viper_si2_uk.qxd.pdf, last access on: 2013/10/09.

Wang XC., Laoui T., Bonse J., Kruth JP., Lauwers B., Froyen L., (2002), 'Direct selective laser sintering of hard metal powders: experimental study and simulation', *International Journal of Advanced Manufacturing Technology*, 19: 351-359.

Williams JM., Adewunmi A., Schek RM, Flanagan CL., Krebsbach PH., Feinberg SE., Hollister SJ., Das S., (2005), 'Bone tissue engineering using polycaprolactone scaffolds fabricated via selective laser sintering', *Biomaterials*, Vol. 26, Iss. 23, pp. 4817-4827.

Xue C., Wang R., Zhang J., Jia S. Tian L.,(2010), 'Growth of ZnO nanorod forests and characterization of ZnO-coated nylon fibers', Materials Letters, Vol. 64, pp. 327-330.

Yuan M, Bourell D., (2012), 'Efforts to Reduce Part Bed Thermal Gradients during Laser Sintering Processing', *Solid Freeform Fabrication Proceedings*, pp. 962-974.

Yuan M and Bourell D., (2013), 'Fundamental Issues for Additive Manufacturing of Lithophanes', *International Conference of Advanced Research in Virtual and Rapid Prototyping*.

Zhang L, Wu D., Chen Y., Wang X., Wan H., Huang C., (2009)'Surface modification of polymethyl methacrylate intraocular lenses by plasma for improvement of antithrombogenicity and transmittance', Applied Surface, Vol. 255, pp. 6840-6845.

Zhang, W., Leu, M.C., Ji, Z. & Yan, Y., 1998. "Rapid Freezing Prototyping with Water", *Proc. SFF Symposium*, Austin TX, pp. 185-192.